Université de Liège

FACULTÉ DES SCIENCES APPLIQUÉES
Unité d'Hydrologie, Hydrodynamique Appliquée
et de Constructions Hydrauliques (HACH)

Année académique 2010

Exchange models for suspended-load in rivers and reservoirs

Mémoire de fin d'études réalisé en vue de l'obtention
du grade d'Ingénieur Civil en construction par

Ludovic Gouverneur

Promoteur : B. Dewals
Composition du Jury : B. Dewals, M. Pirotton, R. Charlier, M. Veschkens

*On parle d'**un** mémoire, de **son** mémoire.*
On est pourtant bien là en face non seulement d'un travail qui en regroupe,
***des** mémoires, comme une construction de souvenirs sur chapitres,*
de ponctuations qui vont bien au-delà du sujet-même,
mais aussi avec une connotation bien plus collective et ouverte,
*et qui fait de mon mémoire aussi le **nôtre**.*
Merci à vous...

Et je tiens avant tout à adresser ce merci à Monsieur Dewals,
mon promoteur, pour m'avoir guidé vers ce sujet passionnant,
pour ses conseils pertinents, la finesse de sa direction et son sourire rassurant.
Je lui suis aussi extrêmement reconnaissant
pour sa présence virtuelle transatlantique, essentielle.

Merci également à l'Université de Belo Horizonte,
au Professeur Palmier et à son équipe, qui m'a accueilli dans son service
avec toute la chaleur brésilienne, l'improvisation aussi...

Merci particulièrement au Professeur Mauro, pour son temps, sa grande
pédagogie et son calme apaisants.

Merci aux Professeurs Pirotton, Charlier ainsi que Monsieur Veschkens qui ont
accepté de juger ce travail, qu'ils entendent bien toute ma gratitude.

Puis merci à vous, mes parents, mes amis, pour votre comprehension
et cet humour que vous avez su garder autour de mes "non" répétés
pendant ces longs moment de sedimentation à mon bureau...

Obrigada à vocês, amigos, Renata, William, Patricia, Jayaram, Bruno,
Guilherme, Igor, Philippe, pela encorajamentos. Não tem que ser ingenerios
para ajudar... "Certos encontros têm este sabor de efêmero. A viajem é o que
torno preciosos os momentos únicos" Isso tambem faz partida deste trabalho.

SUMMARY

UNIVERSITE DE LIEGE
Faculté des Sciences Appliquées
Année académique 2010

Gouverneur Ludovic

Exchange models for suspended-load in rivers and reservoirs

Exchange models are one of the most important aspects for sediment transport models. Poor knowledge about this crucial aspect in sediment transport modeling causes uncertainty and reduces the predictive power of such models.

The adaptation coefficient rules the solid transfer rate between the flow and the river bed. A good knowledge of such a parameter is crucial to model correctly non equilibrium sediment transport.

This master thesis intends to bring a critical comparison of existing adaptation coefficient formulation.

To this end, a literature review describes the theoretical framework of sediment transport. A particular attention is devoted to non-equilibrium exchange models with a focus on four laws describing adjustment process. The laws are described and compared through a sensitivity analysis.

In order to reinforce this critical analysis, a 1D numerical model, using a finite volume approach, has been established to simulate non-equilibrium transport on erodible bed. The latter has been validated confronting it to a wide range of existing literature example including numerical simulations, analytical solutions and laboratory data. It has been demonstrated that the present fully developed model is accurate in modeling channel bed variation under both bed-load and suspended-load transport.

Finally, this powerful tool has assisted the author when comparing the adaptation law along three experiments existing in the literature.

TABLE OF CONTENTS

I. INTRODUCTION

I.1 SEDIMENT ENGINEERING

Events linked to sediments are not trivial. They orient the evolution of rivers, estuaries and coastlines. Above the landscape drawing and the consequences of its morphologic transformations, sediment transport affects the functioning of hydraulic constructions (channel, harbor ...) and reduces their lifetime (e.g. dam reservoirs). The engineer must go through all those events in order to dominate them.

Sedimentation engineering embraces various aspects (planning, analysis ...) to avoid and/or mitigate problems cited above caused by sedimentation processes (erosion, entrainment, deposition ...).

These fluvial processes pose great challenges for river scientists and engineers. Indeed the exposure of the fluvial systems to the natural environment adds to the complexity of understanding the process of sediment transport and the resulting morphological evolution of rivers.

Laboratory experiments to predict sediment transport are generally very time-consuming, and costly. Hence, there is a need for mathematical models capable of predicting sediment transport.

I.2 NUMERICAL MODELS

The quality of the modeling is widely viewed as the key that could unlock the full potential of computational fluvial hydraulics.

Despite the encouraging progress in its development during the last half a century, mathematical river modeling is still a complex but intriguing problem which one can only hope to solve one day. Indeed, predictive power of such models is far for being satisfactory in many situations. In their paper, Cao and Carling (2002) deal with three special issues of mathematical river models:

- Turbulence closure models,
- Calibration and verification/validation,
- Bottom boundary conditions

The latter is discussed as one of the main sources of model uncertainty. Also, it is directly related to modeling of sediment transfer between the bed and the water column, known as *exchange processes*. In other words, *exchange models* are intrinsically defined by the bottom boundary condition.

Depending on the hypothesis made on the bottom boundary condition, the model uses the concepts of equilibrium or non-equilibrium transport which makes a huge difference in many applications.

I.3 SCOPE OF SUBSEQUENT CHAPTERS

The ambition of this master thesis is to make a critical comparison of exchange models existing in the literature. Especially, a great attention is devoted to one of the parameters defining non-equilibrium exchange models, known as the *adaptation coefficient*.

Hence, a 1D numerical sediment transport model has been fully developed in order to provide a powerful tool to reinforce the critic.

Chapter II introduces basic concepts relevant in modeling sedimentation processes while Chapter III proposes a literature review. In this latter chapter, existing models for suspended-load and exchange models are presented with a particular focus on the adaptation coefficient.

Chapter IV presents the assumptions and structure of the model developed. In Chapter V, the model is confronted with existing knowledge for validating sediment transport model.

Finally, the different formulations for the adaptation coefficient are compared in Chapter VI, using the fully developed model.

II. FUNDAMENTALS

II.1 SEDIMENT PROPERTIES

This section briefly defines fundamental parameters for sediment transport modeling such as: rock types, sediment particles size, distribution, density and fall velocity.

II.1.1 ROCK TYPE

The solid phase in sediment transport can be any granular substance. The property of the rock-derived fragments (porosity, size distribution ...), known as “sediments”, all play a role in determining the transportability of the grains under fluid action.

Sediments in the size range of silt or coarse gravel are generally produced by mechanical means, including fracture or abrasion. On the other hand, the clay minerals are produced by chemical actions. Because of their little size and nature, clays display cohesiveness, which makes them more resistant to erosion.

This master thesis, involving suspension mode of sediment transport (see section II.2), deals with fine sediments. Nevertheless, cohesion becomes an issue when very fine sediments are concerned. Also these aspects have not been considered in this paper which is devoted to exchange models for *non cohesive* sediments.

II.1.2 DENSITY AND SPECIFIC WEIGHT OF SEDIMENT

Sediment density, ρ_s, is the mass of sediment per unit volume, often in kg.m^{-3}. It depends on the material of sediment. A common value in sedimentation engineering is 2650 kg.m^{-3} and corresponds to quartz.

The specific weight of sediment, γ_s, is the weight of sediment per unit volume, often in N m^{-3}. It is related to the sediment density by

$$\gamma_s = \rho_s g \qquad \textbf{(Eq II-1)}$$

The specific gravity of sediment, G, is defined as the ratio between the sediment density ρ_s and the density of water ρ_w. For quartz particles, the specific gravity is

$$G = \frac{\rho_S}{\rho_w} = 2.65 \qquad \textbf{(Eq II-2)}$$

II.1.3 SIZE

The size of the particles is a very important notion as it appears in almost all sediment related formulas such as sediment settling velocity, entrainment rate, transport capacity... The notation *d* is used to denote it. The typical units are

- Millimeters [mm] : for sand and coarser material
- Micrometers [μm] : for clay and silt

Different sediment sizes have been suggested: *nominal diameter*, *fall diameter* and finally *sieve diameter*, the most readily available. Each sieve has a square mesh, the gap size of which corresponds to the diameter of the largest sphere that would fit through.

One of the most popular "typical diameters" is d_{50}, known as the median particle size defined in the next section.

II.1.4 SIZE DISTRIBUTION

Any sediment sample normally contains a range of sizes. An appropriate way to characterize these samples is in terms of a grain size distribution. Consider a large bulk sample of sediment of given weight. Let's define $p_f(d)$ as the fraction by weight of material that is finer than size *d*. The customary engineering representation of the grain size distribution consists of a plot of $p_f \times 100$ (percent finer) versus $log_{10}(d)$. In other words, a semi-logarithmic plot is employed (Figure II-1).

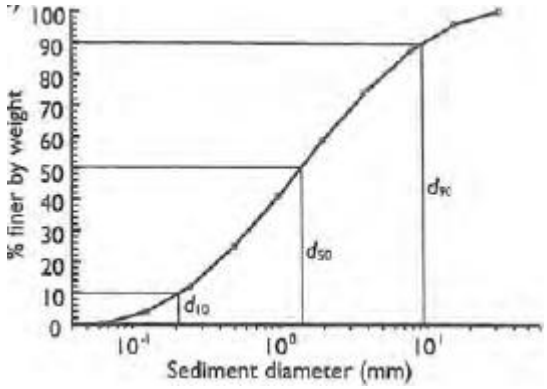

Figure II-1: Particle size distribution (Wu, 2008, p. 15)

Note that the median particle size introduced in the previous section is also represented. It can be now defined as the grain size for which 50% of the bed material is finer.

II.1.5 POROSITY

The porosity *p* quantifies the fraction of a given volume of sediments that is composed of void space:

$$p = \frac{V_{voids}}{V_{total\ space}} \quad \textbf{(Eq II-3)}$$

If a given mass of sediments of known density is deposited, the volume of the deposit must be computed assuming that at least part of it will consist of voids. Consequently, this parameter is important when formulating the evolution of bed morphology.

In the case of well-sorted sand, the porosity can often take values between 0.3 and 0.4. Let's note that in gravel-bed rivers, the finer particles can occupy the spaces between coarser particles, reducing the void ration as low as 0.2.

II.1.6 SHAPE

There are a number of ways to classify grain shape. A simple way to characterize it is in terms of lengths a, b, c of the major, intermediate, and minor axes, respectively. According to the relative importance of theses lengths, the grain can be characterized as a sphere, a rodlike or blade like. This parameter plays a fundamental role when defining the particle fall velocity.

II.1.7 FALL VELOCITY

A fundamental property of sediment particles is their fall velocity or settling velocity.

Falling under action of gravity, a particle will reach a constant, terminal velocity once the fluid drag force on the particle is in equilibrium with the gravity force. The fall velocity of sediment grain in water is determined by its diameter, density, viscosity of the water and particle shape. Indeed, the well known expressions valid for a sphere cannot be applied for natural sediment particle because of the differences in shape. The terminal fall velocity of non spherical sediment particles can be determined from the following formula (van Rijn L. C., 1993, p. 3.13):

(Eq II-4)

$$\omega_s = \frac{(s-1)gd^2}{18\,\nu} \qquad 1 < d \leq 100\ \mu m \quad \textbf{(a)}$$

$$\omega_s = \frac{10\nu}{d}\left[\left(1 + 0.01\frac{(s-1)gd^3}{\nu^2}\right)^{0.5} - 1\right] \qquad 100 < d \leq 1000\ \mu m \quad \textbf{(b)}$$

$$\omega_s = 1.1[(s-1)gd]^{0.5} \qquad d \geq 1000\ \mu m \quad \textbf{(c)}$$

Where *d* is the sieve diameter; *s* is the specific gravity and *ν* is the kinematic viscosity of water.

It is important to note that the fall velocity of a single particle is modified by the presence of other particles. Experiments with uniform suspension of sediments and fluid have shown that the fall velocity is strongly reduced with respect to that of a single particle (van Rijn L. C., 1993).

II.2 SEDIMENT TRANSPORT

The term sediment transport covers a wide range of grain size transported by flowing water, ranging from fine clay particles to large boulders/rocks. They are often viewed in distinct size classes such as fine sand, coarse gravel and so on.

Depending on the *sediment*- (grains size, density), *fluid*- (density, viscosity) and *flow*- (strength and turbulence) characteristics, sediment transport may occur in a variety of modes. In turn, these modes involve different size classes at the same time or the same classes at different times.

In rivers and channels with moderate gradient, there are two systems of classifying transport modes, according to:

1) the sediment size (or source) :
    a. **Bed-material load**: made up of moving sediment particles that are found in appreciable quantity in the channel bed.
    b. **Wash-load**: consists of the finer particles (silt and gray) in the suspended-load that are continuously maintained in suspension by the flow turbulence and that are not found in significant quantities in the bed.
2) the mechanism of transport :
    a. **Bed-load**: the particles roll, slide or saltate along the bed, and never deviate too far from it.
    b. **Suspended-load**: these particles move in suspension and are the part of the load which is not bed-load.

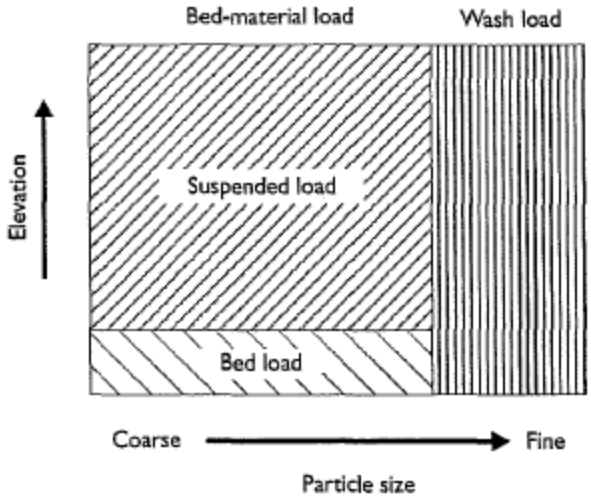

Figure II-2: sediment load (Wu, 2008, p. 18)

Numerical models may deal with one or more components of total sediment transport. In general *wash-load* cannot be predicted by hydraulic-based relationship. Consequently, it is usually not modeled but determined by field measurements.

Along this work, the second system is considered. Under this system, suspended-load consists of the finer sediment maintained in suspension by turbulence, whereas bed-load consists of the

coarser particles transported along the bed intermittently by rolling, sliding or salting (Figure II-3).

The boundary between suspended-load and bed-load transport is not precise and may vary with the flow strength. Indeed, the higher the flow strength, the coarser are the sediment that can be suspended by turbulence. Whatever the flow strength or sediment characteristics, it must be noticed that suspension always occurs with bed-load, while the contrary is not true. Together, bed-load and suspended-load compose the total sediment load.

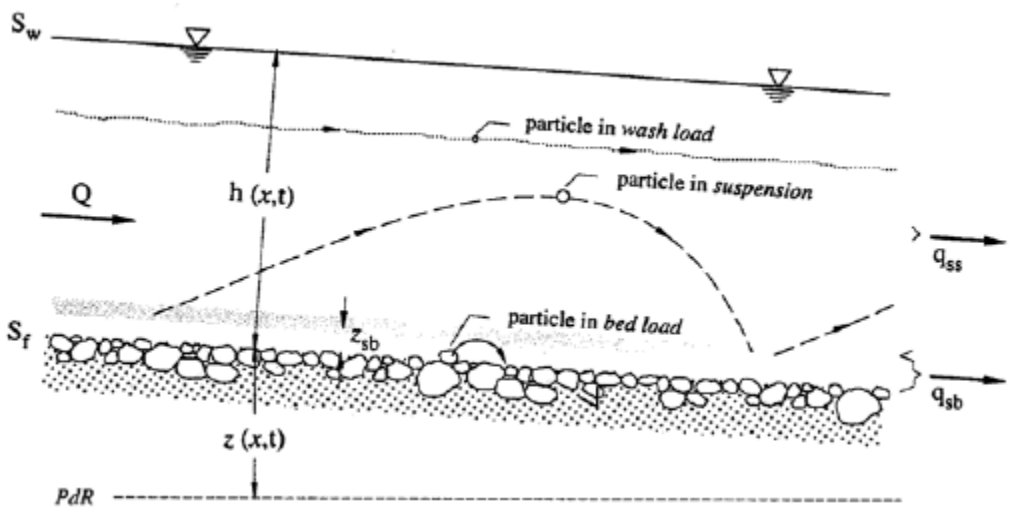

Figure II-3 : Conceptual sediment transport modes (Graf, p. 356)

Some models predict bed-load only and are limited mainly to gravel and coarser sediments. Others predict total sediment load and are unable to account for exchange process between the two layers.

As stated in the introduction, the objective of this master thesis is to study the exchange process between sediment transport and river bed. Consequently, a suspended-load model has been fully developed. As stated before, suspended-load transport is an extreme case of bed-load transport. On account of this, a bed-load model should naturally (yet not necessarily) be computed.

III. LITERATURE REVIEW

III.1 EXISTING MODELS FOR SUSPENDED-LOAD

III.1.1 EQUATION OF SOLID TRANSPORT

The 3-D hydrodynamic set of equations consists of four equations (3 momentum and 1 continuity) and four unknowns (flow velocities and flow depth). The system is usually closed with a flow resistance relation and a turbulence closure model.

In order to describe sediment transport process, a new fundamental variable appears: *c* which is the local suspended-load volumetric concentration. Thus, a new equation is required to close the model. This equation is called the *sediment continuity equation*.

After many hypotheses (flow and particles speed equal in horizontal plane, low sediment concentration, Reynolds' averaging to include turbulence ...), the most widely accepted form of the sediment continuity equation is:

$$\frac{\partial c}{\partial t} + \underbrace{\frac{\partial (uc)}{\partial x} + \frac{\partial (vc)}{\partial y} + \frac{\partial (wc)}{\partial z}}_{advection} - \underbrace{\frac{\partial (\omega_s c)}{\partial z}}_{gravity} = \underbrace{\frac{\partial (\varepsilon_s \partial_x c)}{\partial x} + \frac{\partial \left(\varepsilon_s \partial_y c\right)}{\partial y} + \frac{\partial (\varepsilon_s \partial_z c)}{\partial z}}_{diffusion} \qquad \textbf{(Eq III-1)}$$

Where *u, v, w* are the components of mean velocity in the *x*-, *y*-, *z*- directions; ω_s is the particle settling velocity; ε_s is the dispersion coefficient accounting for both molecular and turbulence diffusion.

III.1.2 DEPTH-AVERAGED MODELS

In this section, the derivation of depth-averaged equations from (Eq III-1) via depth-integrating is addressed. First, a conceptual description of flow and sediment transport is presented. Then, the boundary conditions related to sediment transport are introduced. Finally, the depth-averaged equations are obtained according to their domain of integration.

Conceptual description of flow and sediment transport

As stated in section II.2, bed-load and suspended-load transport behave differently. For this reason the water column is often divided into two zones:

- Bed-load transport layer[1] $z_b < z < z_b+\delta$
- Suspended-load transport layer $z_b+\delta < z < z_s$

where z_b is the bed-elevation[2]; z_s is the water surface elevation and δ is the thickness of the bed-load layer.

[1] Or bottom layer

[2] Subscript *b* denotes that the parameter is considered at the bed level.

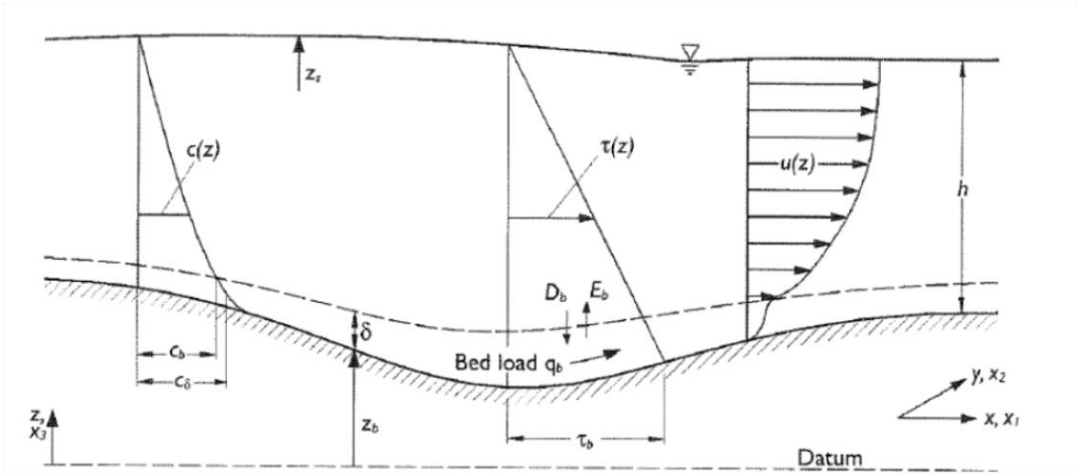

Figure III-1: (Wu, 2008) : Configuration of flow sediment transport

Boundary conditions

In order to perform the integration of (Eq III-1) over the suspended-load transport layer, both upper- (at $z = z_s$) and bottom- (at $z = z_b + \delta$) boundary conditions are required. Indeed, the following expression[3] must be known at both boundaries:

$$\left(\omega_s c + \varepsilon_s \frac{\partial c}{\partial z}\right) \quad \textbf{(Eq III-2)}$$

Similarly to the usual upper *flow* boundary condition, the net vertical sediment flux across the water surface should be zero[4]. Considering the water surface horizontal and according to (Eq III-2), the *upper boundary condition* is expressed as:

$$\left(\omega_s c + \varepsilon_s \frac{\partial c}{\partial z}\right)_{z=z_s} = 0 \quad \textbf{(Eq III-3)}$$

There are usually two approaches to specify the *bottom boundary condition*:

- Concentration boundary condition
- Gradient boundary condition

The descriptions as well as the advantages/disadvantages of both conditions types are detailed in section III.2. For the following developments, the gradient boundary condition is assumed. The latter defines a net entrainment flux:

$$\left(\omega_s c + \varepsilon_y \frac{\partial}{\partial y}(c)\right)_{|_{z_b+\delta}} = D_\delta - E_\delta \quad \textbf{(Eq III-4)}$$

with D_δ the near-bed deposition flux and E_δ the near-bed entrainment flux.

[3] (Eq III-2) is the integrant obtained by projection of (Eq III-1) on the vertical axis, after applying flow boundary condition.

[4] The water free surface is considered horizontal.

Depth-averaged sediment transport equations

The sediment continuity equation, (Eq III-1), could be integrated over both sediment transport layers (Figure III-1). Before performing the integral, let's define *C*, the most important sediment-related fundamental unknown. The depth-averaged suspended-load concentration *C* is defined by

$$C = \frac{1}{h-\delta}\int_{z_b}^{z_s} c\, dz \qquad \textbf{(Eq III-5)}$$

Where *c* is the local suspended-load concentration and (*h*-δ) is the thickness of the suspended-load transport layer (Figure III-1).

<u>Suspended-load layer integration</u>

The three-dimensional sediment transport equation (Eq III-1) is first integrated over the suspended-load zone:

$$\int_{z_b+\delta}^{z_s}\left[\frac{\partial}{\partial t}(c)+\frac{\partial}{\partial x}(uc)+\frac{\partial}{\partial y}(vc)+\frac{\partial}{\partial z}(\omega c)-\frac{\partial}{\partial z}(\omega_s c)\right]dz =$$

$$\int_{z_b+\delta}^{z_s}\left[\frac{\partial}{\partial x}(\epsilon_s\partial_x c)+\frac{\partial}{\partial y}(\epsilon_s\partial_y c)+\frac{\partial}{\partial z}(\epsilon_s\partial_z c)\right]dz \qquad \textbf{(Eq III-6)}$$

Both flow- and sediment- boundary conditions are used to perform the integral**.** In addition the bed-load layer is assumed to be very thin (δ << *h*) and the lag between fluid- and sediment-particles is considered negligible. Using all preceding hypotheses and applying the Leibniz's rule results in:

$$\frac{\partial}{\partial t}(hC)+\frac{\partial}{\partial x}(hUC)+\frac{\partial}{\partial y}(hVC) =$$

$$\frac{\partial}{\partial x}\left[\left(h(\Gamma_s\ \ \partial_x C+D_{sx})\right)\right]+\frac{\partial}{\partial y}\left[\left(h\left(\Gamma_s\ \ \partial_y C+D_{sy}\right)\right)\right]+E_\delta-D_\delta \qquad \textbf{(Eq III-7)}$$

where *C* the mean concentration defined by (Eq III-5); $(\Gamma_s\ \ \partial_x C)$ and D_{si} are the turbulent and dispersion sediment fluxes, respectively.

The integral of the product of two functions is not equal to the product of the integrals. Accordingly, writing

$$\int_{z_b+\delta}^{z_s}\left(\varepsilon_s\partial_{x_i}c\right)\approx h\,\Gamma_s\ \ \partial_{x_i}C \qquad \textbf{(Eq III-8)}$$

is an additional hypothesis. In the model presented in Chapter IV, Γ_s is simply given by the average value along the vertical. Furthermore, for the sake of clarity, Γ_s is rewritten ε_s.

D_{sx} and D_{sy} are the dispersion sediment fluxes and account for the dispersion effect due to the non-uniform distribution of flow velocity and sediment concentration over the flow depth. These fluxes can be written as:

(Eq III-9)

$$D_{sx} = -\frac{1}{h}\int_{z_b+\delta}^{z_s}(u-U)(c-C)dz \qquad \textbf{(a)}$$

$$D_{sy} = -\frac{1}{h}\int_{z_b+\delta}^{z_s}(v-V)(c-C)dz \qquad \textbf{(b)}$$

These terms are sometimes combined with the turbulent diffusion fluxes[5]. Most of the time, they are simply neglected. In both cases the channel is assumed to be straight enough.

According to the preceding hypotheses (Eq III-7) is rewritten as

$$\frac{\partial}{\partial t}(hC) + \frac{\partial}{\partial x}(hUC) + \frac{\partial}{\partial y}(hVC) = \frac{\partial}{\partial x}[h\,\varepsilon_s \partial_x C] + \frac{\partial}{\partial y}\left[h\,\varepsilon_s \partial_y C\right] + E_\delta - D_\delta \qquad \textbf{(Eq III-10)}$$

Bed-load layer integration

The same integration is made over the bed-load zone. The bed-load layer thickness is assumed to be constant. In that case, the bed-variation equation reads

$$(1-p)\frac{\partial}{\partial t}(z_b) + \frac{\partial}{\partial x}(\alpha_{bx}\, q_b) + \frac{\partial}{\partial y}\left(\alpha_{by}\, q_b\right) = -(E_\delta - D_\delta) \qquad \textbf{(Eq III-11)}$$

where p is the porosity; z_b the bed elevation; q_b is the bed-load transport rate by volume per unit time and width (m^2s^{-1}) ; α_{bk} and α_{by} are the direction cosines of bed-load movement.

Depth-averaged 1D model

A section-average 1-D model would be obtained by integration of (Eq III-1) over the cross-section. Nevertheless, the 1-D model studied in this work is simply obtained by neglecting transversal terms in (Eq III-10) and (Eq III-11). In that case, the fundamentals equations describing the sediment transport and evolution of bed morphology are:

The bed variation equation:

$$\underbrace{(1-p)\frac{\partial}{\partial t}(z_b)}_{Unsteady\ bed\ variation} + \underbrace{\frac{\partial}{\partial x}(q_b)}_{Advection} = -\underbrace{(E-D)}_{Net\ entrainment\ flux} \qquad \textbf{(Eq III-12)}$$

The advection diffusion:

$$\underbrace{\frac{\partial}{\partial t}(hC)}_{Unsteady\ concentration} + \underbrace{\frac{\partial}{\partial x}(hUC)}_{Advection} = \underbrace{\frac{\partial}{\partial x}[h\,\varepsilon_s \partial_x C]}_{Diffusion} + \underbrace{E-D}_{Net\ entrainment\ flux} \qquad \textbf{(Eq III-13)}$$

[5] In that case, ε_s is replaced by a mixing coefficient to represent the diffusion and dispersion effects together.

III.1.3 EQUILIBRIUM AND NON-EQUILIBRIUM MODELS

General aspect of equilibrium

For a given situation characterized by sediment properties and flow conditions, the flow can carry a certain quantity of sediment without net deposition or deposition. This is called a dynamic equilibrium state and the flow has reached its sediment-carrying capacity. Net erosion and sedimentation rates are on balance.

When the quantity of sediment supplied is less than the capacity and the riverbed is movable, net erosion may occur. The sediment concentration will then increase until the carrying capacity is reached again. The experiments studied in section V.2 illustrate that phenomenon of adjustment. In the opposite situation, for example in a reservoir (see section V.1.1), deposition is likely to occur.

Relevance with respect to models

Whatever the complexity of the sediment transport model (1-D, 2-D, or 3-D) described in the former section, two governing equations are necessary, namely

- The suspended-load transport equation $f(c)$
- The bed variation equation $f(q_b, \partial z_b/\partial t)$

That being so there are three fundamental sediment related unknowns:

- The suspended-load concentration c
- The bed-load transport rate q_b
- The bed change rate $\partial/\partial t\,(z_b)$

Two approaches exist to close the model, namely the equilibrium- and non-equilibrium sediment transport models.

Equilibrium sediment transport model

In equilibrium models, the flow is assumed to be at its sediment-carrying capacity. The latter is prescribed by a sediment transport functions involving local hydraulic parameters and sediment properties. For instance, for bed-load transport:

$$q_b = q_{b_*}(U, h, d_{50}, \dots) \qquad \textbf{(Eq III-14)}$$

The actual bed-load transport rate (q_b) equals the transport capacity under the equilibrium condition (q_{b*}). One of the major sources of uncertainty with equilibrium models comes with the sediment transport function (q_{b*}) that must be introduced to determine sediment transport rate or discharge.

For suspended-load, a similar formulation could be used to express q_s, the suspended-load transport rate, leading to the same uncertainty.

Non-equilibrium transport model

"Because of variations in flow and channel properties, the sediment transport in natural rivers usually is not in states of equilibrium. (…) the assumption of local equilibrium is usually unrealistic and may have significant errors …" (Wu, 2008)

This excerpt underlines the importance of non-equilibrium models. They are at least intuitively more advanced than equilibrium models.

Indeed, they account for the limited availability of sediment under specific conditions. In addition, they account for the temporal and spatial lag between flow and sediment transport. In other words they consider the time and space required for sediment transport to adapt to its transport capacity in line with the local flow conditions.

For only bed-load the commonly accepted formulation is:

$$(1-p)\frac{\partial z_b}{\partial t} = \frac{1}{L_b}\left(q_b - q_{b_*}\right) \quad \textbf{(Eq III-15)}$$

where L_b is the adaptation length of bed-load. For only suspended-load transport, the bed change is attributed to the net sediment flux at the lower boundary of the mixing layer:

$$(1-p)\frac{\partial z_b}{\partial t} = \alpha\omega_s(C - C_*) \quad \textbf{(Eq III-16)}$$

with α the adaptation coefficient; C_* the equilibrium depth averaged concentration; C the depth-averaged concentration. Let's note that the (Eq III-16) can also be written as:

$$(1-p)\frac{\partial z_b}{\partial t} = \frac{1}{L_s}\left(q_s - q_{s_*}\right) \quad \textbf{(Eq III-17)}$$

With L_s the adaptation length for suspended-load transport defined as:

$$L_s = \frac{Uh}{\alpha\omega_s} \quad \textbf{(Eq III-18)}$$

The adaptation lengths, L_b and L_s , are characteristic distances for sediment to adjust from non-equilibrium to equilibrium transport.

This master thesis studies the effect of α (or L_s) on suspended sediment transport. For this reason, (Eq III-16) is extensively used in this work. The theoretical framework of this formulation is exposed in detail in sections III.2 and III.3.

III.2 BOTTOM BOUNDARY CONDITION

"Prescribing the near-bed boundary condition for suspended-sediment computation, i.e, defining the sediment-exchange processes, has proven to be one of the most challenging problems in mobile bed modeling."(Spasojevic & Holly, 2008, p. 707)

As stated in section III.1.2, the vertical sediment flux is zero at the free surface. In contrast, two kinds of bottom (or near-bed) boundary conditions exist: the *concentration* and the *gradient* boundary condition. Both of them are herein described and compared.

III.2.1 CONCENTRATION BOUNDARY CONDITION

In their paper, Galappatti and Vreugdenhil (1985) resume the different ways to consider the concentration boundary condition. The general approach consists in assuming an expression of the concentration near the bed:

$$c_\delta = c_\delta(u_*, h \dots) \quad \textbf{(Eq III-19)}$$

The function could be for example an empirical formulation in terms of the local bed shear stress. The most commonly accepted approach is the assumption that c_δ corresponds to the equilibrium concentration:

$$c_\delta = c_{\delta_*} \quad \textbf{(Eq III-20)}$$

with c_{δ_*} being the equilibrium sediment concentration at δ over the bed (Figure III-1). Thus, near the bed, the concentration adjusts immediately to local equilibrium whereas higher along the depth, a slower adjustment occurs.

III.2.2 GRADIENT BOUNDARY CONDITION

The other approach defines a net entrainment flux ($E_\delta - D_\delta$). It is based on the relative value between two opposite fluxes:

- Sediment deposition flux (downward) D_δ
- Sediment entrainment flux (upward) E_δ

By contrast with (Eq III-20) the near-bed concentration c_δ remains the near-bed actual concentration and constitutes the deposition flux defined as:

$$D_\delta = \omega_s(c)_{z=z_b+\delta} = \omega_s c_\delta \quad \textbf{(Eq III-21)}$$

in which c_δ is the suspended-load concentration at the interface between the suspended-load and bed-load zone ($z = z_b + \delta$).

The upward flux is widely defined as being the capacity of flow picking up sediment under the considered flow conditions and bed configuration:

$$E_\delta = -\left(\varepsilon_s \frac{\partial c}{\partial z}\right)_{z=z_b+\delta} \quad \textbf{(Eq III-22)}$$

In equilibrium state, the erosion flux would equal the deposition flux, which yields:

$$E_\delta = D_\delta \quad \textbf{(Eq III-23)}$$

Inserting (Eq III-21) and (Eq III-22) in (Eq III-23) gives:

$$\left(\varepsilon_s \frac{\partial c}{\partial z}\right)_{z=z_b+\delta} = \omega_s c_{\delta_*} \quad \textbf{(Eq III-24)}$$

Thus, in the gradient boundary condition, the upward flux E_δ is related to the equilibrium near-bed concentration. This relation is extended to the non-equilibrium situations to express the near-bed *net* entrainment flux as:

$$E_\delta - D_\delta = \omega_s (c_{\delta_*} - c_\delta) \quad \textbf{(Eq III-25)}$$

In this approach, the sediment exchange is defined as the difference between the upward sediment entrainment flux *E* and the downward sediment deposition flux *D*. The net entrainment flux has opposite signs in the governing equations for the bed-load (Eq III-11) and (Eq III-10) for suspended-load transport.

III.2.3 COMPARISON

Armanini & Di Silvio (1986) gave three arguments against the use of the concentration boundary condition.

1) The downward flux should physically depend on the actual amount of sediment present in the water stream.
2) When the stream is strongly overloaded, the concentration profile near the bed should display an unrealistic positive gradient in the upward direction.
3) If the concentration boundary is used, $\varepsilon_s \, \partial c/\partial z$ depends on the actual concentration profile. However, the turbulent fluctuations, which control the entrainment of the particles, are basically unaffected by the actual transport of sediment (if the concentration is reasonably law).

In addition, as stated in section III.1.2, the concentration boundary condition makes the strong assumption of equilibrium sediment transport at the interface of the two transport layer. This treatment is not adequate for non-equilibrium conditions.

On the other hand, the gradient boundary condition leads to a consistent formulation of exchange processes which applies for both equilibrium and non-equilibrium sediment transport. Indeed the near-bed net entrainment flux is proportional to the difference between actual and equilibrium near-bed concentration. Consequently, in equilibrium state no exchange occurs and $E_\delta = D_\delta$.

Therefore, the latter condition is more general than the concentration boundary condition and is used for the present developed model.

III.3 EXISTING EXCHANGE MODELS

As stated in the introduction, the actual poor knowledge concerning the exchange models seriously limits the predictive power of sediment transport models.

After a short overview of the different types of exchanges models (3D or depth-averaged), problematic parameters are isolated. A particular attention is devoted to the adaptation coefficient given this is the topic of most interest of the work.

III.3.1 INTRODUCTION

"Generic to any spatially dimensional mathematical river models, formulating the net flux of sediment exchange with bed material is of fundamental importance for fluvial sediment transport".(Z.Cao, 2002)

This excerpt expresses the importance of the present chapter, and more widely, of this work. Mathematically, the net entrainment flux is formulated by $(D_\delta - E_\delta)$, which comes from the hypothesis made on the bottom boundary condition (see section III.2).

Indeed, in section III.1.2, the gradient boundary condition, given its applicability for modeling equilibrium and non-equilibrium situation, is presented as the most general formulation to represent exchange processes between both bed-load and suspended-load layers. This choice results in

$$D_b - E_b = \omega_s \left(c_\delta - c_{\delta *}\right) \qquad \textbf{(Eq III-26)}$$

In the 3D models, this formulation is directly applicable provided a near-bed transport capacity law is used.

However, in the depth-averaged (2-D or 1-D) models, the near-bed concentration, c_δ, defining the deposition flux is not a dependent variable anymore. The following sections present the different ways to challenge this problem.

III.3.2 DEPOSITION FLUX

In order to avoid the determination of c_δ, the *deposition flux* D_δ is usually determined by relating c_δ to the depth-averaged suspended-load concentration C through

$$D_b = \omega_s c_b = \omega_s \alpha_c C \qquad \textbf{(Eq III-27)}$$

in which α_c is the adaptation coefficient for deposition.

III.3.3 ENTRAINMENT FLUX

Specifying bed sediment entrainment flux is the key to determinate the net exchange flux. For modeling the *entrainment flux* E_b, two general approaches exist, namely models using:

1) An near-bed capacity formula: $E_b = \omega_s c_{b_*}$
2) An average capacity formula: $E_b = \alpha_{c*} \omega_s C_*$

where $c_{\delta*}$ is the equilibrium near-bed concentration; C_* is equilibrium depth-averaged concentration and α_c is the adaptation coefficient for entrainment, under equilibrium conditions.

The former formulation assumes that E_δ can be determined directly using an empirical formula for $c_{\delta *}$ while the latter uses a similar approach as for deposition flux. The fact remains that C_* have to be determined using a depth-averaged empirical formula[6].

III.3.4 NET ENTRAINMENT FLUX

Using the average capacity formula leads to the coherent relation:

$$D_\delta - E_\delta = \alpha_c \omega_s C - \alpha_{c*} \omega_s C_* \quad \textbf{(Eq III-28)}$$

Thus, the near-bed concentrations c and $c_{\delta*}$ have been linked to the depth-averaged concentrations C and C_* thanks to the adaptation coefficients α_{c*} and α_c. However the difference is often assumed to be negligible (Wu, 2008). Consequently, the net exchange flux is defined by:

$$D - E = \alpha \omega_s (C - C_*) \quad \textbf{(Eq III-29)}$$

Where α is a new general adaptation coefficient[7].

III.3.5 MAIN ISSUES ON MODELING THE ENTRAINMENT FLUX

The net entrainment flux is formulated by (Eq III-29). That equation exposes all the parameters needed to implement exchange processes between the bed-load and suspended-load layers.

The depth-averaged concentration C doesn't pose any problem as it is a model dependent variable.

The particle settling velocity (see section II.1.7) can be approximated by the settling velocity of a single particle in many situations or be adapted, taking into account the sediment concentration.

However the problem of determining C_* and α has actually not been solved. Both could be described by many laws. It has to be noted that this master thesis focuses on α, the adaptation coefficient. Section III.4.2 lists different formulations for α, which are compared in Chapter VI using the developed model.

---

[6] Another way consists in integrating a suspended-load concentration profile using a near-bed capacity formula. This approach leads to another problem as δ remains to be defined as well as a Rous-Type number.

[7] A brief development leads to the conclusion that α is usually less than the two coefficients α_c and α_{c*}.

III.4 ADAPTATION COEFFICIENT

After introducing general aspects relevant to understand the complexity of the adaptation coefficient determination, some formulations are first presented. Based on this literature review, the relevant parameters are isolated and the formulations are compared.

III.4.1 GENERAL ASPECTS

Adaptation coefficient includes a wide range of definitions. Neither precise value nor expression is fully commonly accepted. It may cover erosion, deposition or both, according to the author hypotheses. It may refer to a single value (or a set of values) or be a semi-analytical expression.

Complexity of the adaptation coefficient

Theoretical value

Theoretically, α_c and α_{c*} defined in section III.3.4 are used to link the near-bed concentration to the depth-averaged concentration:

$$D_\delta - E_\delta = \alpha_c \omega_s C - \alpha_{c*} \omega_s C_* \quad \textbf{(Eq III-30)}$$

As the concentration (in equilibrium state or not) is always higher near the bed, the resulting values of α should always be superior to 1.

$$\alpha_c = \frac{c_b}{C} > 1 \; and \; \alpha_{c*} = \frac{c_{b*}}{C_*} > 1 \quad \textbf{(Eq III-31)}$$

As stated before, a single value is often used for simplicity. However, this theoretical definition doesn't always reflect the reality. Many factors herein summarized should be understood in order to correctly interpret some in situ or laboratory based determination of α.

Settling velocity effects

The settling velocity ω_s is often set from prediction formulae valid for a single particle in still water. This is only valid for low sediment concentrations. However, the effects of sediments concentration on ω_s should be considered in most situations. Furthermore, only the action of drag forces and submerged weight are usually considered. Other forces related to moving water also influence the settling velocity (e.g. turbulent stresses).

These effects, if not considered when calculating ω_s, should be lumped in the adaptation coefficient value. That correction may lead to a significant reduction of the value of α.

Bedform effects

Despite they are always present in natural rivers, little is known about the effects of bedforms on sediment transport. In some formulations, they affect the thickness of the bed-load layer, increasing its value. As shown in the sensitivity analysis conducted in section III.4.3, this effect also reduces the value of α.

.

Cross-sectional shape

Zhou and Lin (1998) demonstrated that in cross-sectional-averaged 1-D models, the value of α depends on the cross-sectional shape. However, in the case of the developed 1-D model where only streamwise effects are considered in rectangular flumes, this effect doesn't influence the value of α.

Numerical value VS semi analytical formulation

A method is still needed to determine α for the general purpose of sediment transport. In case of natural rivers, the adaptation coefficient can be treated as a coefficient of calibration. Han (1980) (cited by (Wu, 2008)), made tests in many rivers and reservoirs and suggested that α is about 1 for strong erosion, 0.5 for mild erosion and deposition, and 0.25 for strong deposition in 1-D models. It remains that theses values are mostly applicable for each situation considered. Thus, calibrating α using measurement data is preferable for each specific case study.

In some typical situations, α could be expressed by a semi-analytical law. These laws mainly depend on the type of boundary conditions used to integrate the 3-D equations for sediment transport (see section III.2) and also on the hypothesis made concerning the bottom layer thickness.

III.4.2 FORMULATIONS AND CHARACTERISTICS

Armanini & Di-Silvio (1988)

By depth-averaging the 2-D equation for suspended transport, Di Silvio & Armanini (1981) obtained an expression for the characteristic length L_s by assuming a semi-empirical formulation for the vertical concentration profile. This expression is represented by curve 1 in Figure II-1 where the non-dimensional length $L^*\omega/Uh$ (or $1/\alpha$) is given as a function of the sediment number ω/u_*.

Galappatti and Vreugdenhil (1985) derived a function (curve 2) through an approximate analytical integration of the pure vertical 2-D advection-diffusion equation. They used the concentration boundary condition (see section III.2).

The concentration profile used was based on the parabolic-constant distribution[8] of the diffusion coefficient suggested by DHL (1980). The velocity distribution was based on a logarithmic profile:

$$u = \frac{u_*}{\kappa} ln\left(\frac{z}{z_0}\right) \qquad \textbf{(Eq III-32)}$$

With z_0 the zero-velocity distance;

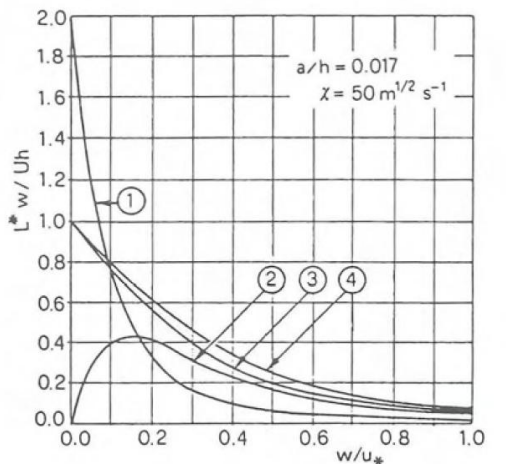

Figure III-2: Characteristic length of particles transported in suspension, following different integration procedures along the vertical (Armanini & Di Silvio, 1988)

Armanini and Di Silvio (1986) obtained curve 3 by the same integration except that a gradient boundary condition was used. Indeed, they argued that the concentration boundary condition may result in large errors for fine sediments (see section III.2).

In addition they applied the procedure of Galappatti and Vreugdenhil directly to the transport (cu) instead of to the concentration (c). By prescribing again a gradient boundary condition, they obtained an expression represented by curve 4, practically identical to curve 3.

[8] The zero order profile for concentration has about the standard shape as originally derived by Rouse (1937)

An approximate equation that fits curve 4 is the following:

$$L_{adim} = \frac{1}{\alpha} = \frac{\delta}{h} + \left(1 - \frac{\delta}{h}\right) exp\left[-1.5\left(\frac{\delta}{h}\right)^{-\frac{1}{6}} \frac{\omega_S}{u_*}\right] \quad \textbf{(Eq III-33)}$$

in which ω_s is the settling velocity (see section II.1.7), u_* is friction velocity, δ is the thickness of the bottom layer.

Armanini and Di Silvio (1986) defined δ, the thickness of the bottom layer as the distance from the bed surface above which the assumed closure model for turbulence is fully valid. They assumed that this distance is equal to the Nikuradse's roughness of the bed (Di Sivio & Armanini, 1981):

$$\delta = 33\, z_0 = 33h\, /exp\, (1 + \frac{\kappa C_{Chézy}}{\sqrt{g}}) \quad \textbf{(Eq III-34)}$$

$C_{Chézy}$ is the Chézy resistance of the channel expressed by (Eq IV-6)

Armanini and Di Silvio (1986) interpreted that equation stating that the thickness of the bottom layer has the order of magnitude of the grain diameter when the bed is flat, and the order of magnitude of the bed form height in the presence of bed forms. However, for flat bed, this value was considered too small. A minimum value of 0.05h was then advised.

In Figure III-3, the curve represents the variation of α for a fixed value of $\eta_\delta = 0.05$.

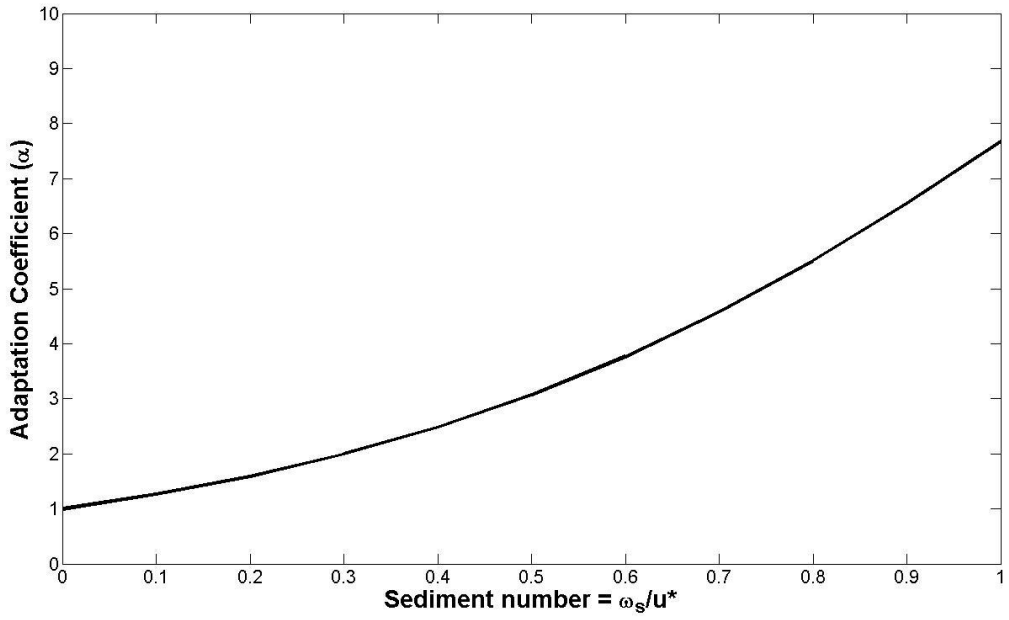

Figure III-3: Armanini and Di Silvio (1986)'s adaptation coefficient

General observations:

- The values increase as the ω/u_* increases
- The values are always larger than 1

Zhou & Lin (1995)

A formula for α was also established by Zhou and Lin (1995) using the analytical solution of the pure vertical 2-D advection-diffusion equation.

A steady, uniform flow was considered as well as a constant diffusivity. As stated in Zhou and Lin (1998), for 1-D rectangular channel, the adaptation coefficient may be taken as identical to that for the depth-averaged 2D cases.

They used the concentration boundary condition for erosion case, and that with the gradient boundary condition for deposition case. The analytical solutions in both cases were expressed as series. These series were then approximated by only one term with small truncation errors. Replacing these approximated solutions into the advection-diffusion, the following solution is obtained:

$$\alpha = \frac{R}{4} + \frac{\sigma_1^2}{R} \qquad \textbf{(Eq III-35)}$$

with $R = \frac{6}{\kappa}\frac{\omega}{u_*}$ (R is a Rouse-type number) and σ_1 is the first root of the following expression:

for erosion: $tg(\sigma_1) = -\frac{\sigma_1}{R}$ for deposition : $2ctg(\sigma_1) = \frac{2\sigma_1}{R} - \frac{R}{2\sigma_1}$

Both erosion and deposition curves are computed in Figure III-4.

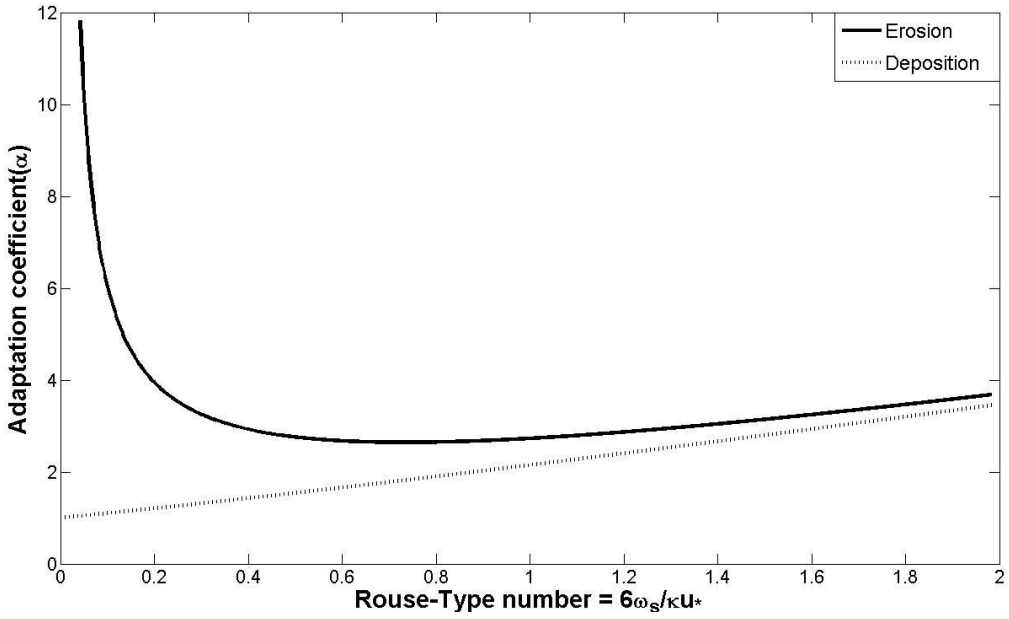

Figure III-4: Zhou & Lin (1995)'s adaptation coefficient

General observations:

- The value of α is always larger than 1.
- The value of α for erosion differs from that for deposition.
- The deposition curve increases linearly while the erosion curve decrease non-linearly
- This function does not depend directly on the bed-load layer thickness.
- The difference between these two curves is significant for small ω/u_*, but gradually decreases as ω/u_* increases.

Let's recall that the adaptation coefficient rules the length needed to reach equilibrium in non-equilibrium situation. Thus, this shows that for small ω_s/u_* it takes a much shorter distance for concentration profiles to approach equilibrium in the case of erosion than in deposition.

Lin & al. (1983)

Lin and al. (1983) presented basic equations resulting from small concentration approximation for a rectangular channel with alluvial bed. That formulation used the basic definition of the adaptation coefficient (Eq III-31).

For fine sediments with sediment number $u_*/\omega_S < 0.1$, C was considered equal to the concentration at the mid-depth.

In order to calculate δ, the thickness of the bed-load layer, Einstein (1977)'s suggestion was assumed. Consequently $\delta = 2d$ with d the grain diameter of sediment. In addition, C was supposed equal to the concentration at mid-depth. On account of these two hypotheses, α was expressed using (Eq III-38) for the concentration distribution, which gives:

$$\alpha = \frac{c_\delta}{C} = \frac{c|_{z=2d}}{c|_{z=h/2}} = \left(\frac{h-2d}{2d}\right)^{Z_R} = \left(\frac{1}{\eta_\delta} - 1\right)^{Z_R} \qquad \textbf{(Eq III-36)}$$

with Z_R is a Rouse-type number defined in section III.4.3. Figure III-5 represents the variation of α with respect to Zr for η_δ = 0.002. This latter value represents a bed characterized by d = 1 mm under a flow with h = 1 m. It has to be noted that the domain computed respects the domain of validity of (Eq III-36).

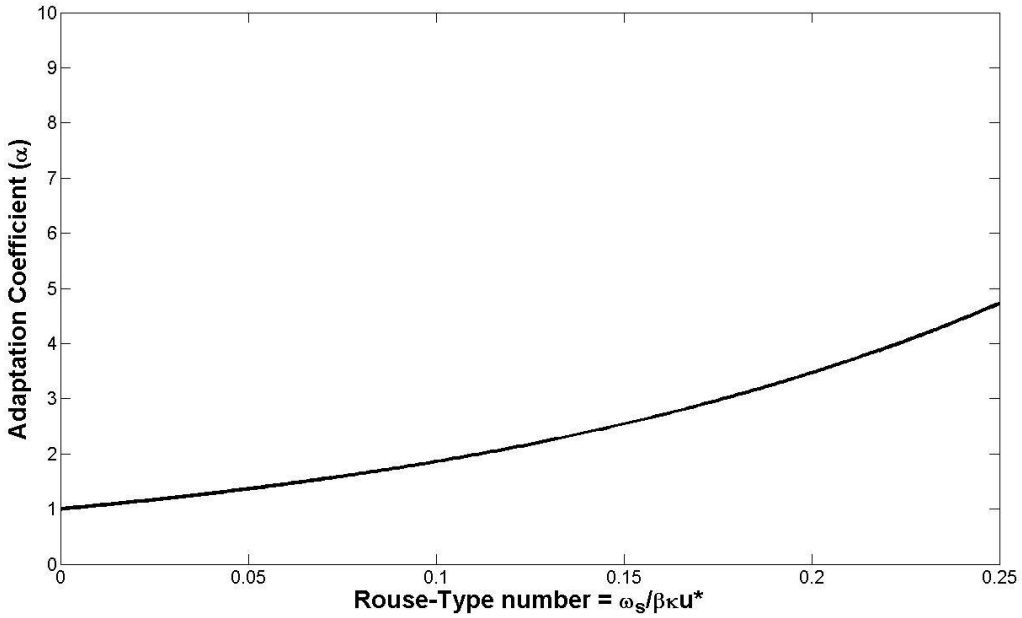

Figure III-5: Lin & al. (1983)'s adaptation coefficient

General observations:

- The values increase as ω/u_* increases.
- The values are always larger than 1
- For $Z_R = 0$, $\alpha = 1$

The adaptation increases far more quickly with respect to the Rouse-Type number than Armanini & Di-Silvio's law. This should be related to the reference depth chosen which is by far lower in this case, increasing the value of α as defined by (Eq III-31).

Guo & Jin (1999)

Similarly to Lin and al. (1983)'s method, Guo and Jin (1999) also used the definition of α to find an analytical solution. However, the depth-averaged concentration was calculated according to the following definition:

$$C = \frac{1}{U}\int_{\eta_\delta}^{1} c\, u\, d\eta \qquad \textbf{(Eq III-37)}$$

Where c and u are the local sediment concentration and flow velocity, respectively. The chosen concentration profile was derived by Rouse (1937):

$$\frac{c}{c_\delta} = \left[\frac{1/\eta - 1}{1/\eta_\delta - 1}\right]^{Z_R} \qquad \textbf{(Eq III-38)}$$

where η is the relative flow depth; η_b is the reference relative flow depth; c and c_δ are the local concentrations which correspond to η and η_b respectively, and z_R is the Rouse number.

The chosen *velocity distribution* was derived from the Prandtl's mixing length theory (Simons & Senturk, 1992) and formulated as:

$$u = U\left[1 + \frac{\sqrt{g}}{\kappa C}(ln\,\eta + 1)\right] \qquad \textbf{(Eq III-39)}$$

Both concentration and velocity profiles were established in equilibrium situations. In reality, under non-equilibrium conditions, they are different from those in the equilibrium state. However, for most alluvial rivers with fine sediments, the vertical distributions of suspended sediment concentrations in the two states are not significantly different ((Lin, Huang, & Li, 1983) cited by (Guo & Jin, 1999)).

Hence, α can be considered to be approximately the same for both equilibrium and non-equilibrium states and be evaluated assuming the system is in equilibrium. Inserting (Eq III-38) and (Eq III-39) in (Eq III-37), the following formulation for α was obtained:

(Eq III-40)

$$\alpha = \left(\frac{1}{\eta_\delta} - 1\right)^{Z_R}\left[\left(1 + \frac{\sqrt{g}}{\kappa C_{Chézy}}\right)\int_{\eta_\delta}^{1}\left(\frac{1}{\eta} - 1\right)^{Z_R} d\eta + \frac{\sqrt{g}}{\kappa C_{Chézy}}\int_{\eta_\delta}^{1}\left(\frac{1}{\eta} - 1\right)^{Z_R} ln\,(\eta)\, d\eta\right]^{-1}$$

For η_δ , the values recommended were [0.005-0.01]. Figure III-6 shows the evolution of α with respect to the Rouse-type parameter Z_R for the Chezy coefficient $C_{Chézy}$ = 36.0 and $\eta_\delta = 0.01$

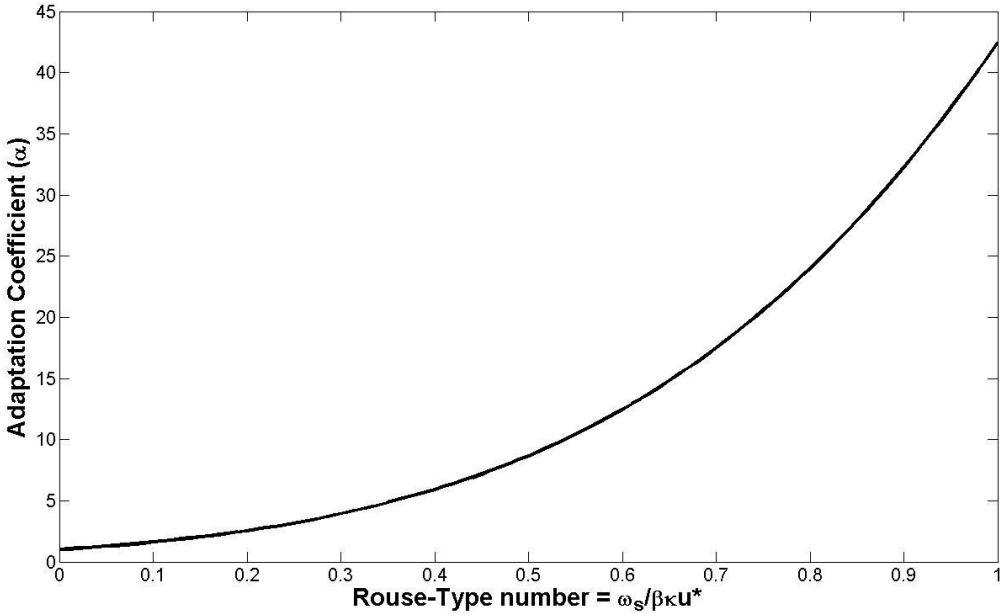

Figure III-6: Guo & Jin (1999)'s adaptation coefficient

General observations:

- The values increase as the ω/u_* increases.
- The values are always larger than 1
- For $Z_R = 0$, $\alpha = 1$

These observations are the same as for Lin & al.'s law. However, the field of application is not limited to small values of Z_R.

The expression can be used to approximately estimate the value of the adaptation coefficient for the case of fully developed flow with suspended sediment. This is the case when flow at the inlet is fully mixed with suspended sediment and the bed has enough sediment to be erodible.

Summary

The following Table III-1 summarizes the preceding considerations.

	Formulation	Rouse-type number	Bottom layer thickness
Armanini & Di-Silvio (1988)	$L_{adim} = \frac{1}{\alpha} = \eta_\delta + (1-\eta_\delta)\, exp\left[-1.5(\eta_\delta)^{-\frac{1}{6}}\frac{\omega_S}{u_*}\right]$	$\frac{\omega_S}{u_*}$	$\delta = 33\, z_0 = 33h\ /exp\ (1 + \frac{\kappa C_{Chézy}}{\sqrt{g}})$
Zhou & Lin (1995)	$\alpha = \frac{R}{4} + \frac{\sigma_1^2}{R}$ with for erosion: $tg(\sigma_1) = -\frac{\sigma_1}{R}$ for deposition: $2ctg(\sigma_1) = \frac{2\sigma_1}{R} - \frac{R}{2\sigma_1}$	$R = \frac{6}{\kappa}\frac{\omega}{u_*}$	---
Lin & al. (1983)	$\alpha = \left(\frac{1}{\eta_\delta} - 1\right)^{Z_R}$	$Z_R = \frac{\omega_s}{\beta\kappa u_*}$	$\delta = 2d_{50}$
Guo & Jin (1999)	$\alpha = \left(\frac{1}{\eta_\delta} - 1\right)^{Z_R}\left[\left(1 + \frac{\sqrt{g}}{\kappa C_{Chézy}}\right)\int_{\eta_\delta}^{1}\left(\frac{1}{\eta} - 1\right)^{Z_R} d\eta + \frac{\sqrt{g}}{\kappa C_{Chézy}}\int_{\eta_\delta}^{1}\left(\frac{1}{\eta} - 1\right)^{Z_R} ln\,(\eta)\, d\eta\right]^{-1}$	$Z_R = \frac{\omega_s}{\beta\kappa u_*}$	Value suggested: [0,005-0,01]

Table III-1

III.4.3 SENSITIVITY ANALYSIS

The sensitive parameters are isolated in each one of the 4 laws described in the former section:

- Armanini & Di-Silvio (1988) — $f(u_*, \omega_s, \eta_\delta\ (h, C_{Chézy}))$
- Zhou & Lin (1995) — $f(u_*, \omega_s)$
- Lin & al (1983) — $f(u_*, \omega_s, \eta_\delta\ (d))$
- Guo & Jin (1999) — $f(u_*, \omega_s, C_{Chézy}, \eta_\delta)$

The sediment representative diameter, *d*, is an essential parameter in sediment modeling and is the basis in any sediment related study (see section II.1.4).

The *Chézy* coefficient can be determinate via (Eq IV-6).

The ratio u_*/ω_s, also called sediment number, and η_δ, the relative bottom layer thickness are common to all formulations[9]. The sensibility of the adaptation laws to these parameters is studied in detail in the next paragraphs.

Bottom layer thickness

"The surface that separates suspension and bed-load transport is as much arbitrary as the same definition of the two modes of transport". (Armanini & Di Silvio, 1988)

As stated in section III.4.2 Zhou and Lin's law is totally independent of δ, the bottom layer thickness. On the contrary, the other three adaptation laws are highly dependent of that parameter. For these latter, the influence of δ (or $\eta_\delta = \delta / h$) on α is qualitatively the same. Figure III-7 illustrates the behavior of Guo & Jin's law, for $C_{Chézy} = 36$.

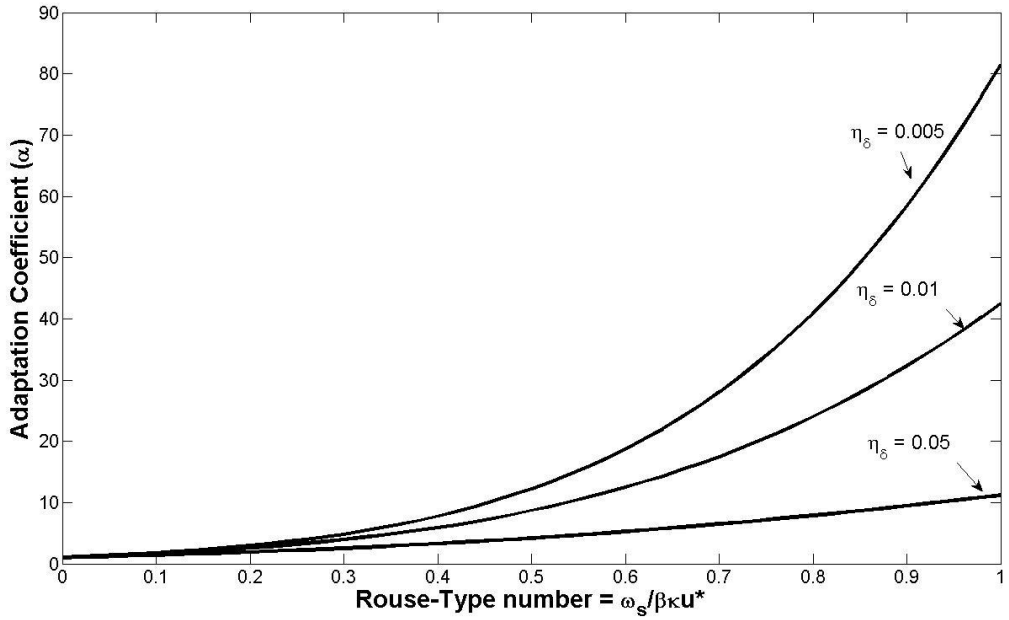

Figure III-7: Sensitivity of Guo & Jin's law to the relative reference depth η_δ

[9] Except η_δ for Zhou & Lin's law

When the value of $\omega/\beta\kappa u_*$ remains constant, α decreases quickly with an increase in reference depth, δ_b. This is in agreement with the general observations that sediment concentrations vary suddenly with a small depth from the bottom. The smaller the value of δ, the larger the ratio c_δ/C which defines the adaptation coefficient.

Sediment parameter

In Armanini & Di-Silvio's law, the ratio u_*/ω_s appears "alone" while in the other laws, it is often linked to κ and β to form a Rouse-Type number:

- Zhou & Lin (1995) $R = \frac{6\omega_s}{\kappa u_*}$
- Lin & al (1983) and Guo & Jin (1999) $Z_R = \frac{\omega_s}{\beta\kappa u_*}$

where β is a constant over the flow depth that describes the difference of diffusion between discrete sediment particle and a fluid particle.

Since the exponent Z_r is expressed in terms of an unknown parameter β, an additional equation is necessary for solving α. Van Rijn's (1984) formulated it as:

$$\beta = 1 + 2\left(\frac{\omega}{u_*}\right)^2 \quad for \quad 0.1 < \frac{\omega}{u_*} < 1 \qquad \textbf{(Eq III-41)}$$

Guo & Gin (1999) used another definition for β by changing the domain of validity of van Rijn's formula:

(Eq III-42)

$$\beta = 1 \qquad \text{for } \frac{\omega}{u_*} < 0.1 \qquad \textbf{(a)}$$

$$\beta = 1 + 2\left(\frac{\omega}{u_*}\right)^2 \qquad \text{for } 0.1 < \frac{\omega}{u_*} < 0.707 \qquad \textbf{(b)}$$

$$\beta = 2 \qquad \text{for } \frac{\omega}{u_*} > 0.707 \qquad \textbf{(c)}$$

Using (Eq III-42 b) yields:

$$Z_R = \frac{\omega}{\beta\kappa u_*} = \frac{1}{\kappa}\left(\frac{\omega}{u_*}\right)\left[1 + 2\left(\frac{\omega}{u_*}\right)^2\right]^{-1} \qquad \textbf{(Eq III-43)}$$

Wu (2008, p. 47) computed and compared Armanini & Di-Silvio's law with Zhou & Lin's law. This analysis is widened to Guo & Jin and Lin & al's law. Figure III-8 contains the variation of the different adaptation coefficients with respect to the sediment number, considering $\eta_\delta = 0.017$.

From Figure III-8, and from all the previous observations (section III.4.2), it could be noticed that:

1) The adaptation coefficient is always larger than one.
2) Except for Zhou & Lin's erosion curve, the general behaviour is an increase of α with the sediment parameter.
3) For small sediment parameter values, Armanini & Di-Silivio's function is very close to Zhou & Lin's law for deposition. The difference increases as the sediment parameter increases.
4) The same observation is valid for Guo & Jin's function with respect to Lin & al's expression.

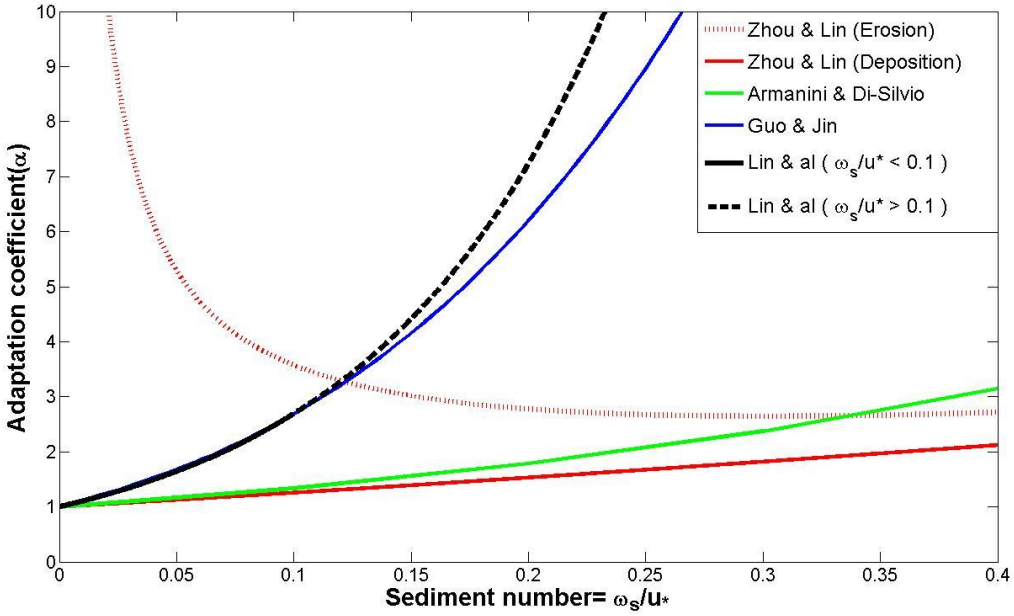

Figure III-8: Comparison of the adaptation laws

The first observation is consistent with the definition of α as given in section III.4.1. Indeed, the near-bed concentration is always higher than the depth-averaged concentration.

Furthermore, for a flow transporting coarser particles, i.e. higher ω_s and higher sediment parameter, the near-bed concentration is larger with respect to the depth-averaged concentration. That leads to a larger value of α.

Both Armanini & Di-Silivio's and Zhou & Lin's functions were derived for a pure vertical 2-D case. To perform that integration, the gradient boundary condition (see section III.2.2) was used in both integrations[10] which explain the similarity between the green curve and the red one.

On the contrary, a concentration boundary condition was used in Zhou & Lin's law for erosion. As a result, the curve for erosion may have large errors for fine sediment (i.e. small sediment parameter), as discussed by Armanini and Di Silvio (1986).

Guo & Jin's and Lin & al's functions are derived from the definition of α itself. However, different hypothesis were assumed concerning the determination of the depth-averaged concentrations[11]. Lin & al.'s hypothesis leads to a restriction of the domain of validity for α. That limitation is represented by both continuous and dashed black curves.

.

[10] Only for erosion in Zhou & Lin's integration

[11] It must be noted than the bottom layer thickness is defined in Lin & al's law while in Guo & Jin's function δ (or η_δ) must be estimated or calibrated.

IV. FLOW AND SEDIMENT TRANSPORT MODEL

IV.1 CONCEPTUAL MODEL

Along this work, a 1D numerical model has been developed in order to compute the transport of sediments and the evolution of the bed morphology caused by sediment transport (Figure III-1). The model is based on the Reynolds-averaged Navier-Stokes equations, subsequently depth-integrated, on an advection-diffusion equation for the suspended sediments, and on the Exner equation for the bed-load transport.

Bed-load and suspended-load sediment transport are coupled by the net entrainment sediment flux (*E*-*D*) across the borders between the two transport layers.

In order to close the model, an equilibrium approach is used to determine the bed-load transport rate as well as the entrainment flux *E*. Thus, empirical laws are required to provide instantaneous value for bed-load transport capacity and suspended sediment carrying capacity.

In addition, a non-equilibrium approach is used for exchange processes between bed-load and sediment-load transport layers. As a result, mass transfer is based on the net entrainment flux and on the adaptation coefficient which characterizes the rate at which the new carrying capacity is attained.

The model is non-coupled which means that the model is preferably applied to long term simulations.

The proposed model intends to be as predictive as possible in the sense that nearly only the basic hydrodynamic parameters (depth, current velocity) and the basic sediment- (ρ, $d50$, $d90$) and bed-(p) characteristics need to be known.

Discretization of the equation relies on a finite volume scheme over a uniform one-dimensional grid. The numerical fluxes at each finite volume boundaries are determined by a flux vector splitting that exploits the physical characteristics of the flow.

Finally, the mathematical model, its discretization and its implementation into a computational code are assessed by comparison with experimental, numerical and analytical data.

IV.2 MATHEMATICAL DESCRIPTION

IV.2.1 GOVERNING EQUATION

Mean-flow equations

Using the Reynolds-averaged and depth-integrated flow equations, the 1-D partial differential equations for steady flow with hydrostatic pressure distribution in a rectangular channel can be written as:

$$\frac{\partial hBU}{\partial x} = 0 \qquad \textbf{(Eq IV-1)}$$

$$\frac{\partial}{\partial x}\left(hU^2 + g\frac{h^2}{2}\right) - \left(S_0 - S_j\right) = 0 \qquad \textbf{(Eq IV-2)}$$

where B is the channel width; h is the flow depth; U is the depth-average velocity; g is the gravitational acceleration; S_0 is the bed-slope term which expression is $gh\,\partial z_b/\partial x$, with z_b being the bed elevation and S_j is the channel flow resistance term determined by $S_j = ghJ$ with J the friction-slope. This hydrodynamic set of equation is closed using one of the flow resistance laws presented in section IV.2.2.

Advection-diffusion equation for suspended sediment transport

The 3D Reynolds-averaged sediment continuity equation is integrated over the flow-depth. The transversal terms are then neglected. This results in the 1D advection-diffusion formulation. The latter describes the transport of the depth-averaged concentration in suspended-load C. This equation in which the dispersion sediment fluxes[12] are neglected reads:

$$\frac{\partial}{\partial t}(hC) + \frac{\partial}{\partial x}(hCU) = \frac{\partial}{\partial x}\left(\varepsilon_s h\frac{\partial C}{\partial x}\right) + (E - D) \qquad \textbf{(Eq IV-3)}$$

where ε_s is the dispersion coefficient. The first term of the right-hand side accounts for longitudinal diffusive transport while the second represents the net entrainment flux. The latter accounts for solid exchange between the bed-load and the suspended-load layers.

Bed variation equation

The 1-D bed variation equation results from the same integration over the bed-load transport layer (see section III.1.2), that is:

$$(1-p)\frac{\partial}{\partial t}(z_b) + \frac{\partial}{\partial x}(q_b) = -(E - D) \qquad \textbf{(Eq IV-4)}$$

where p is the porosity and q_b is the bed-load transport rate by volume per unit time and width (m^2s^{-1}). The first term of the left-hand side represents the bed elevation changes caused by bed-load transport gradient and exchanges processes.

[12] The dispersion fluxes account for the dispersion effect due to the non-uniform distribution of flow velocity and sediment concentration over the flow depth (see section III.1.2)

IV.2.2 ASSUMPTIONS

Non coupled model

The proposed model is non-coupled which means that time scale of bed evolution is low with respect to the response of the flow to the changing bed configuration. On account of this, the model is therefore preferably applied to long term simulations.

The assumption implies two phases in the model calculation. The water surface curve and all related flow characteristics are first calculated. Next, constant flow parameters are used to evaluate the bed deformation.

Flow resistance

In order to close the hydrodynamic model, a flow resistance relation must be provided. In the model, both Manning's and Chézy's laws are implemented.

Chézy's law is expressed as follows:

$$U = C_{Chézy}\, {R_h}^{1/2} i^{1/2} \quad \textbf{(Eq IV-5)}$$

where $i = \partial z_b / \partial x$ is the bed slope and $C_{Chézy}$ is the Chézy coefficient given by

$$C_{Chézy} = 18\, log\left(\frac{12\, R_h}{k_s}\right) \quad \textbf{(Eq IV-6)}$$

Manning's law is formulated as

$$U = \frac{1}{n} {R_h}^{2/3} i^{1/2} \quad \textbf{(Eq IV-7)}$$

where *n* is the Manning's coefficient.

Dispersion coefficient

In order to close the set of equation constituting the model, a turbulent closure model is necessary. Many formulations using parabolic profile and/or involving additional differential equations exist. Betchler and Schrimpf (1988) found that the vertical distribution of the dispersion coefficient ε_s has no significant influence on the settling rates.

It was then suggested to use a depth-averaged value of ε_s for the calculation of many practical sediment transport problems. Thus, ε_s is simply given by:

$$\varepsilon_s = \frac{\kappa}{6} u_* h \quad \textbf{(Eq IV-8)}$$

where κ is the von Kármán constant which is assumed to be κ=0.41 and u_* the shear velocity given by:

$$u_* = g^{0,5} \left(\frac{U}{C_{Chézy}}\right) \quad \textbf{(Eq IV-9)}$$

Boundary conditions

The upper boundary condition assumes that the net vertical sediment flux across the water surface is zero while a gradient approach (see section III.1.2) is used for the bottom boundary condition:

$$E_\delta - D_\delta = w_s(c_{b_*} - c_b) \quad \textbf{(Eq IV-10)}$$

with E_δ and D_δ being respectively the near-bed entrainment- and deposition fluxes; $c_{\delta*}$ and c_δ respectively correspond to the equilibrium- and calculated near-bed concentrations; ω_s is the fall velocity as define by (Eq II-4).

Further, as the near-bed concentrations are not averaged values, (Eq IV-10) is rewritten as:

$$E - D = \alpha\, \omega_s(C_* - C) \quad \textbf{(Eq IV-11)}$$

where C_* and C respectively correspond to the equilibrium and depth-averaged concentration; α is the adaptation coefficient. In order to determine C_*, a sediment carrying capacity must be provided.

Sediment carrying capacity

As stated in section III.3, many formulations exist to express the sediment carrying capacity. Yet none is fully satisfactory. Wuhan (1959)'s formula expresses C_* (kg/m³), the equilibrium averaged concentration (or sediment carrying capacity), as:

$$C_* = k\left(\frac{U^3}{h\omega_s}\right)^m \quad \textbf{(Eq IV-12)}$$

where U is the mean flow velocity; ω_s is the particle settling velocity; h is the flow depth; k and m are coefficients. This formulation is chosen for two reasons.

First this law gives an equilibrium depth-averaged concentration. Many other laws provide equilibrium near-bed concentrations that are defined for different bed-load layer thickness. An assumed concentration profile must then be integrated in order to get the required mean value. Furthermore, in many cases, the concentration profile obtained from the near-bed value is calibrated with measured data. The Rouse-Type number is therefore used to obtain the desired profile. This procedure involving many assumptions is complex and can be source of error.

Second, this formulation offers a good compromise between prediction and calibration. Originally, both coefficients k and m were used to calibrate the law. Guo & Jin (2001) established a relation for k using Bagnold (1966)'s formula as:

$$k = \frac{\gamma\gamma_s}{\gamma_s - \gamma}\frac{(1-e_b)e_s}{C_{ch\acute{e}zy}{}^2} \quad \textbf{(Eq IV-13)}$$

where γ and γ_s are the specific weight of clear water and sediment; e_b and e_s are the bed-load and suspended sediment transport efficiencies. Based on laboratory data, Bagnold (1966) suggested that $(1\text{-}e_b)\, e_s = 0.01$, for straight channel[13].

Finally, m may be estimated from (Eq IV-12) if the equilibrium concentration is known. Given its predictive quality, this formulation is used in the model.

[13] For natural rivers, Rubey (1933) suggested a value of 0.025 for this coefficient.

IV.3 NUMERICAL DISCRETIZATION

IV.3.1 FORMULATION

For the purpose of discretizing the differential equations introduced in the former section, the finite volume method has been used. This method is indeed known to ensure a strict conservativity when applied to conservation laws. In this method, equations are integrated over a finite volume (Figure IV-1). The terms appearing in the integral form of the equations are converted to surface integrals by using the divergence theorem. These terms constitute fluxes *f* at the surfaces of each finite volume[14].

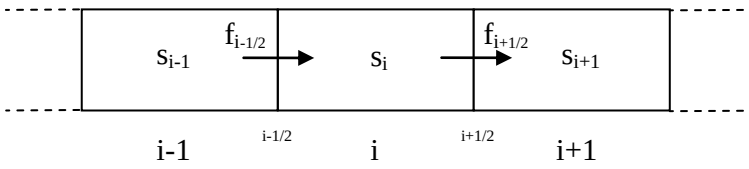

Figure IV-1 : Finite volume grid

Because the flux entering in a given volume is identical to the one leaving the adjacent volume, this method is strictly conservative when applied to a conservative formulation:

$$\frac{\partial s}{\partial t} + \frac{\partial}{\partial x}(f) = S \qquad \textbf{(Eq IV-14)}$$

where *s* is the conservative unknown; *f* is the general flux and *S* represents the source term. For the sake of clarity, Table IV-1 gives the value of these various terms for the model of sediment transport.

	Equation	***s***	***f***	***S***
0	Continuity for water	*1*	hU	*0*
1	Momentum for water	*1*	$hU^2 + \frac{1}{2} + gh^2$	$-gh(\frac{\partial z_b}{\partial x} - J)$
2	Advection-Diffusion for suspended sediment	*hC*	$f_{3_{adv}} + f_{3_{diff}} = hCU + \varepsilon_s\, h\, \partial C/\partial X$	*E-D*
3	Bed-Load transport and Bed variation	$(1-p)\, z_b$	q_b	*-(E-D)*

Table IV-1: Conservative form of equations

[14] The subscript *i* designates the centre of the finite volume while $i \pm 1/2$ denotes the finite volume boarder.

IV.3.2 PSEUDO-UNSTEADY FLOW

Using a pseudo-time stepping method constitutes a good strategy to solve equation in the Table IV-1. Solution is obtained when a steady regime appears in the following equation:

$$\beta_n \frac{\partial h}{\partial \tau} + \frac{\partial}{\partial x}\left(hU^2 + g\frac{h^2}{2}\right) - gh\left(\frac{\partial z_b}{\partial x} - J\right) = 0 \qquad \textbf{(Eq IV-15)}$$

IV.3.3 TIME DISCRETIZATION

In order to ensure a good convergence, the time-integration of the model is performed by a Runge-Kutta31B algorithm. This approach provides indeed an excellent compromise between considerable internal dissipation and a little restrictive stability condition. This scheme relies on the canonical form of (Eq IV-14):

$$\frac{\partial \boldsymbol{s}}{\partial \boldsymbol{t}} = \boldsymbol{L}[\boldsymbol{s}] \qquad \textbf{(Eq IV-16)}$$

with *L* being the differential spatial operator for each equation of Table IV-1: Conservative form of equations

The Runge-Kutta method is given by the following equations:

(Eq IV-17)

$$s^{(1)} = s^t + \Delta t\, L[s^L] \qquad \textbf{(a)}$$

$$s^{(2)} = s^t + \Delta t\, L\left[s^{(1)}\right] \qquad \textbf{(b)}$$

$$s^{t+1} = s^t + \Delta t\left\{a_0 L[s^t] + a_1 L\left[s^{(1)}\right] + a_2 L\left[s^{(2)}\right]\right\} \qquad \textbf{(c)}$$

Where s^t and s^{t+1} denote respectively the known value of *s* at time *t* and unknown value of *s* at time *t+1*; $s^{(1)}$ and $s^{(2)}$ are both sub-step of Runge-Kutta method characterized by a_0 =0.15, a_1 =0.45 and a_2 =0.4 for Runge-Kutta31B scheme.

IV.3.4 TIME STEP

Stability analysis provides restrictive conditions on the time step of the computational scheme. Indeed, Von Neuman method shows that the maximum time step directly depends on the maximum eigenvalue λ^{max} of the discretized and linearized spatial operator. It must satisfy the following stability condition:

$$\Delta t \leq \frac{R_0}{\left|\lambda_{max}^{discr}\right|} < \frac{R_0 \Delta x}{\left|2\lambda_{max}^{exact}\right|} \qquad \textbf{(Eq IV-18)}$$

where λ_{max}^{exact} is the biggest eigenvalue of the linearized spatial operator and R_0=1.533 is the radius of Runge-Kutta31B scheme stability curve. Obviously, stability of each equation requires the knowledge of the eigenvalues of the system. This issue is treated in the next section.

The bed elevation calculation time step requires more attention given that both bed-load and suspended-load rates are advected. To satisfy (Eq IV-18) the most restrictive condition must be chosen:

$$|\lambda_{max}| = max\ \left(|\lambda_{max}^{BL}|, |\lambda_{max}^{SL}|\right) \qquad \textbf{(Eq IV-19)}$$

IV.3.5 SPACE DISCRETIZATION

Space discretization relies on a classic finite volume method, which consists in two steps.

The first step consists in reconstructing the values of unknowns at the boundaries of the finite volume. For this purpose, the values at the centre of the meshes are extrapolated up to the boundaries. Consequently, two values are attributed at each boundary.

The second step consists in computing a numerical flux with these two values. In this thesis, the physical flux is applied to one of the two values, called the decentred value. The choice of this value is based on the sign of the celerity.

To illustrate the method, the conservation equation is rewritten as a typical linear advection equation:

$$\frac{\partial s}{\partial t} + \frac{\partial f(s)}{\partial x} = S \qquad \rightarrow \qquad \frac{\partial s}{\partial t} + c(s)\frac{\partial s}{\partial x} = 0 \qquad \textbf{(Eq IV-20)}$$

where the celerity is defined as $c(s) = df/ds$.

Since source term *S* does not affect the sign of the characteristic velocity, it is neglected.

If the celerity is positive, the information propagates from the left to the right. The left side is called upwind and right side downwind. On the opposite, the information propagates from the right to the left if the celerity is negative. The left side is called downwind and the right side upwind.

Clearly, the decentred value must be chosen from where the information comes. The numerical flux is thus upwinded. It can be shown that this approach is stable. However, it requires determining the value of the celerity for each model.

Pseudo-unsteady hydrodynamic model

The only terms which are concerned by the linearization in order to determine the celerity are those that contains derivative of the basic unknown h. The linearization of the momentum equation yields:

$$\frac{\partial h}{\partial \tau} - \frac{1}{\beta_n}(u^2 + gh)\frac{\partial h}{\partial x} = 0 \qquad \textbf{(Eq IV-21)}$$

According to (Eq IV-20), the celerity of this equation is given by:

$$c_h = gh\frac{1-Fr^2}{\beta_n} \qquad \textbf{(Eq IV-22)}$$

With *Fr* the Froude number defined as $Fr = u/\sqrt{gh}$ for rectangular channel. The sign of c_h is discussed in Table IV-1 in relation with the value of the Froude number and the parameter β_n. It shows that the sign of the celerity depends directly on the sign of β_n. However, this parameter was introduced to simplify the shallow-water model. It is still necessary to fix its value.

	$Fr < 1$	$Fr > 1$
$\beta_n > 0$	$c_h > 0$	$c_h < 0$
$\beta_n < 0$	$c_h < 0$	$c_h > 0$

Table IV-1

The value of β_n must be determined. The 1D shallow-water model (see Table VI-1) has two different eigenvalues. Their signs determine two different regimes. If both celerities have the same sign, all the information propagates downstream. It is a super-critical regime characterized by a Froude number greater than one.

On the opposite, information propagates both upstream and downstream in a sub-critical regime (Fr < 1). Eigenvalues have opposite signs. In order to keep the same direction of propagation of the information in the pseudo-unsteady model, the celerity must be positive for Fr > 1. Consequently, the parameter β_n must be negative. Further, β_n does not influence the scheme dispersive characteristics. Thus, according to Table IV-1, the value is simply β_n= -1.

Based on this choice of the value for the parameterβ_n, the numerical flux is computed with the upstream value of the water height h if the Froude number is greater than 1 and with the downstream value of the water height h if the Froude number is lower than 1.

Unsteady bed variation equation

The same procedure is applied to the bed variation equation. The celerity is then given by:

$$c_b = \frac{1}{1-p}\left(-\frac{dq_b}{dh}\right)\frac{1}{1-Fr^2} \qquad \textbf{(Eq IV-23)}$$

where dq_b/dh is determined by derivation of the bed-load transport relation chosen. For given flow conditions, raising the flow-depth value involves decreasing the value of bed-load capacity. This means that dq_b/dh is always negative. As a result, the sign of c_b only depends on the value of Fr as explained by Table IV-2

	Fr < 1	Fr > 1
Cb	> 0	< 0

Table IV-2

As pointed out by Table IV-2, the information of topography z_b propagates downstream if the Froude number is lower than one and upstream otherwise. Consequently, the decentred value of the bed-load flux q_b is the upstream value in sub-critical regime and downstream in super-critical regime. It is the exact opposite of the previous equation.

Unsteady advection-diffusion equation

The only advective flux derivation leads to

$$c_s = U \qquad \textbf{(Eq IV-24)}$$

with U being the mean-flow velocity. (Eq IV-24) means that c_s is positive whatever the flow regime. As a consequence of that, the decentred value is always the upstream reconstructed value.

Note that the diffusive flux, $(\varepsilon_s\, h\, \partial C/\partial X)$, is not advected like bed-load and suspended-load fluxes. Consequently, this term is not linearized and thus doesn't influence the celerity values.

Summary and boundary conditions

Table IV-3 summarizes the sign of the celerities in each model according to the value of the Froude number. As pointed above, these signs determine directly the value of the numerical flux. The latter one is indeed given by the physical flux computed from the upwinded value.

	Celerity	***Fr* < 1**	**Boundary condition**	***Fr* > 1**	**Boundary condition**
Momentum for water	c_h	< 0	Downstream	> 0	Upstream
Bed-Load transport and Bed variation	c_b	> 0	Upstream	< 0	Downstream
Advection-Diffusion for suspended sediment	c_s	> 0	Upstream	> 0	Upstream

Table IV-3

The signs given in Table IV-3 also determine the nature of the required boundary conditions.

In a super-critical flow ($Fr > 1$), one must impose both the water height and the suspended sediment concentration at the upstream boundary as well as the topography (or the bed-load sediment flux) at the downstream boundary.

In a sub-critical flow, one must impose both the suspended sediment concentration and the topography (or the bed-load sediment flux) at the upstream boundary as well as the water height at the downstream boundary.

Most of the time, sediment experiment and studies concern sub-critical flow. In the next section, detailing the algorithmic implementation, the flow is then considered sub-critical.

IV.4 ALGORITHMIC IMPLEMENTATION

To start the computation, the initial conditions (z_{b0}, h_0, C_0 at t = 0) are given for all grid points. The boundary conditions (q, q_b, C at inlet and the value of h at outlet) are given for all time steps. These stored values numerically represent the first-(inlet) and last-(outlet) grid limits.

The algorithm is computed as follows:

1) **Water flow routine**: h_i

   h_i is calculated iteratively till the convergent solutions for water flow is obtained. Both flow boundary conditions h_{out} and q_{inl}[15] are used[16].

2) **Time step**: Δt

   According to flow and sediment characteristics Δt, the time-step, is calculated[17].

3) **Exchange model parameters :** C_{*i} and α_i

   The components of exchange process term (*E-D*), that is C_{*i} and α_i, respectively the equilibrium averaged concentration and the adaptation coefficient are evaluated.

4) **Reconstruction**: 2 value for $f_{i\pm1/2}$

   h_i and C_i are reconstructed in both finite volume edges : $h_{i\pm1/2}$ and $C_{i\pm1/2}$. From this values, the advective fluxes $f_{1,i\pm1/2}$ (= q_b) and $f_{2,i\pm1/2}$ (= hCU) are calculated.

5) **Upwinding**: a single value for $f_{i\pm1/2}$

   In each cell edge, a single value for each advective flux is chosen according to the related celerity sign (see Table IV-3). Note that a single value of the diffusion flux f_{2d} can be obtained at each grid edge given that they don't depend on the sign of the characteristic speeds.

6) **Balance**: z_b^{t+1} and C^{t+1}

   Values of z_b and C are calculated for the next time step (or sub-step).

---

[15] Subscrit "out" in h_{out} and "inl" in q_{inl} denote respectively $h_{N+1/2}$ and $q_{1-1/2}$

[16] Given that bed elevation is susceptible to be modified after each time step, the total elevation (bed + flow depth) is fixed by the boundary condition. Thus the boundary flow depth is adapted at each beginning of the routine.

[17] This calculus only occurs in the first Rung-Kutta time step.

V. MODEL VERIFICATION

The unsteady bed variation equation, including *only* bed-load transport, is first applied to theoretical *reservoir case* as well as to *von Needham et Hey* flume experiment. On both cases, the transport is considered to be at equilibrium.

Then the unsteady advection-diffusion equation is widely validated. Each term (erosion, deposition, advection and diffusion) are tested separately.

Finally, the full sediment transport model detailed in the former section is tested by application to the case the moving trench, which is a well-known standard benchmark test.

V.1 UNSTEADY BED VARIATION EQUATION

V.1.1 LONG TIME SCALE SIMULATION: RESERVOIR

This part of the model has been tested in a typical case of reservoir. The dam created a backwater curve extending to a certain upstream distance. Thanks to the hydrodynamic model, the back water calculation enables the knowledge of the hydraulic parameters (average velocity, water depth ...). As explained in Chapter IV, these parameters are necessary to begin each bed variation calculation loop.

In this experience, a sub-critical flow evolves over a movable bed river. The river bed is composed of quasi-uniform sediments (ρ = 2650 kg/m³) with an average grain size of d_{50} = 6 mm and a porosity of p = 0.3. The Manning coefficient is determined as being n = 0.032 [$m^{-1/3}s$].

In order to calculate the solid transport, the well known Meyer-Peter and Muller law is implemented:

$$\frac{q_b}{\sqrt{(s-1)gd^3}} = 8\left[\frac{R_h\,\xi_M\,J}{(s-1)d} - 0.047\right]^{3/2} \qquad \textbf{(Eq V-1)}$$

where q_b is the bed-load transport rate; s is the specific gravity (2.65); d is the representative particle size diameter (d_{50}); R_h is the hydraulic radius and ξ_M is a roughness parameter (usually $1 > \xi_M > 0.35$), depending on the presence of bedforms.

The unit fluid discharge is kept constant at q = 2.5 m²/s. The other two boundary conditions needed are given by the dam which keeps the water at 23.5 m and an equilibrium bed-load rate given by (Eq V-1) at the upstream end. According to hydraulics parameters, the latter is given by $q_b = 1.69\ 10^{-5}$ m²/s.

The time simulation is 20 years and the domain length is 120 km with Dx = 600 m.

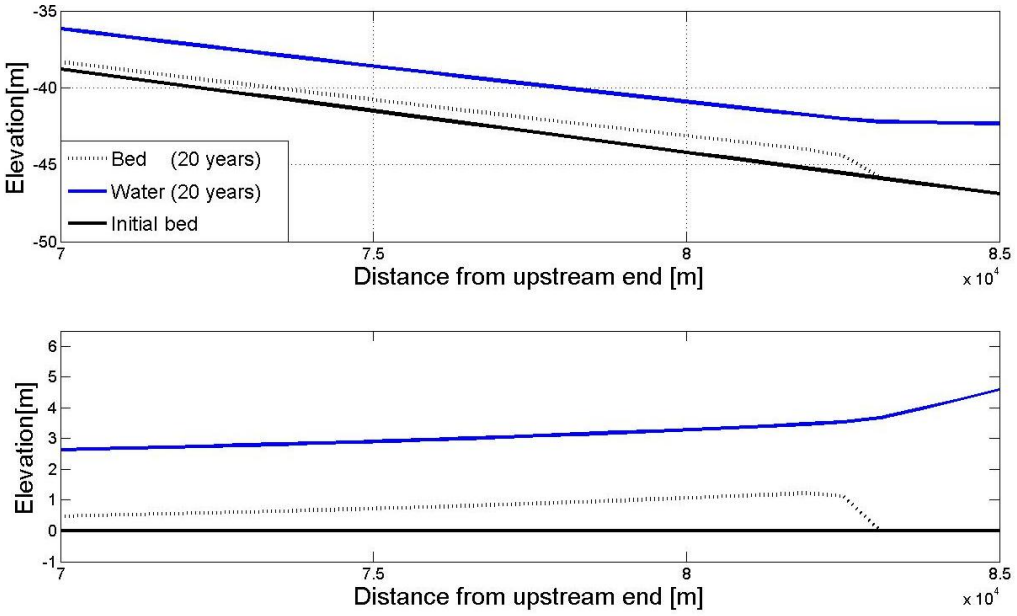

Figure V-1 : Reservoir simulation

The deposition of the sediment, namely the delta formation, is shown in Figure V-1 after 20 years of simulation. The resulting height of the delta is h_δ = 1.2283 m. This value is compared with Minor et al. (1999) which found h_δ = 1.23 m. This long time scale application demonstrates perfect agreement with numerical results from the literature.

V.1.2 SHORT TIME SCALE SIMULATION

This experience shows the consequences of a sudden change in bed-load transport rate. The experiment is described by Figure V-2. Flume experiments permitted to establish a simple bed-load transport relation for this particular case:

$$q_b = (6.06 \;\; 10^{-5})\, U^{1.97} \qquad \textbf{(Eq V-2)}$$

with *U* being the mean flow velocity.

Initially a uniform flow transports sediment at equilibrium. In other words neither deposition nor erosion processes appears. Then a sudden increase in solid transport supply at the upstream end is performed. This results in an immediate net sediment deposition.

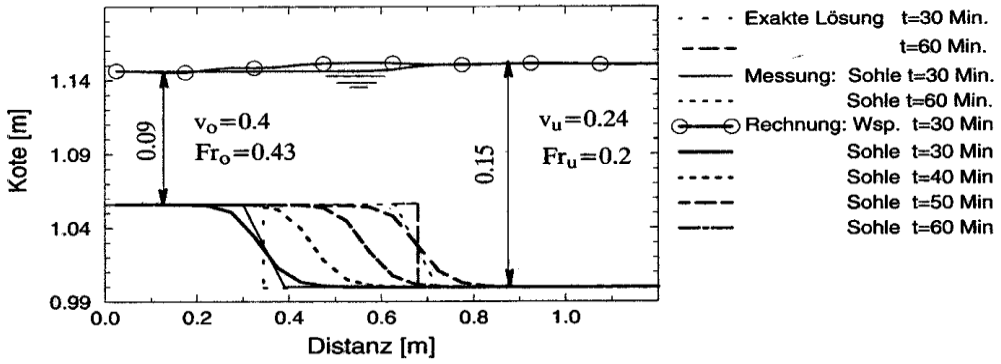

Figure V-2 : Von Needham and Hey experience (Fäh, 1997)

The simulation duration is 60 min and results are also given after 30 min. As can be seen on Figure V-3, the computed results are identical to Figure V-2.

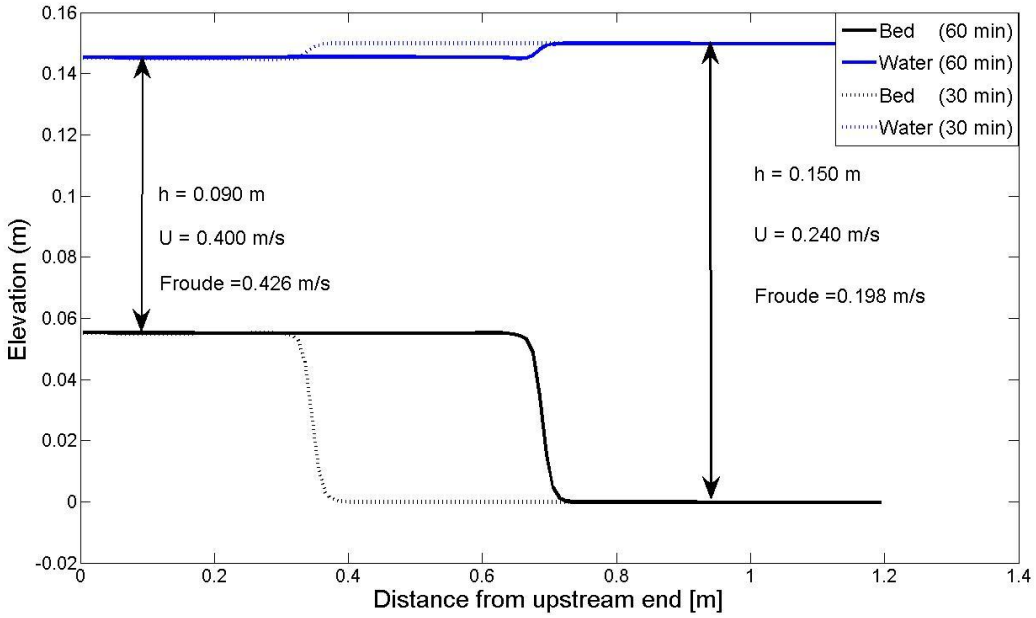

Figure V-3 : Von Needham and Hey : Computed results

Both preceding simulations showed the ability of the model to represent bed variation and bed-load transport for short and long time scale processes. Nevertheless, the transport is always considered to bed at equilibrium. Non equilibrium exchange process between bed-load and suspended-load layers are not taken into account yet.

V.2 UNSTEADY ADVECTION-DIFFUSION EQUATION

This section is devoted to the suspended-load transport model, mathematically described by the advection-diffusion equation. The numerical model is confronted to three particular situations, where non equilibrium transport is underlined.

V.2.1 PERFORATED BOTTOM EXPERIMENT

Experimental configuration

The first experiment was realized by Wang and Ribberink (1986). The flume experiment consisted in discharging sand into a flume with initially rigid bottom. The sediment concentrations were then measured in a steady, uniform flow. The experimental configuration is sketched on Figure V-4.

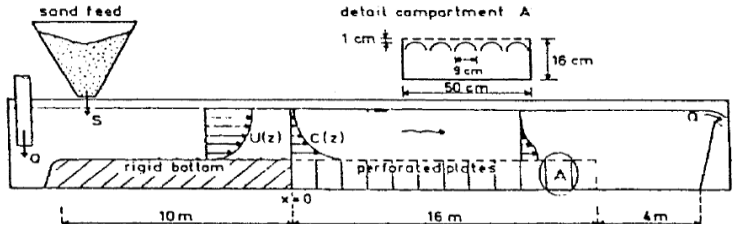

Figure V-4 : Case with perforated bottom: Experimental configuration

The rigid part of the channel allows the flow to develop both concentration and velocity equilibrium profiles. A perforated bottom was used to trap the sediment particles in contact with the bed. Indeed the sediments reaching the bottom could not be re-entrained. The upstream reference ($x = 0$) is set at the downstream end of the rigid bottom part of the channel. The full set of data necessary to run the simulation is given in Table V-1.

	Characteristics	Values		Units
Flow	Water depth	h	= 0.215	m
	Flow velocity	U	= 0.56	m/s
Sediments	Size	D_{50}	= 0.095	mm
		D_{90}	= 0.105	mm
	Fall velocity	w_s	= 0.0065	m/s
	Density	ρ	= 2650	kg/m³
	Roughness height	k_s	= 0.0025	m
	Inlet concentration	C_0	= 125	mg/L
Channel (sand bed)	Length	$L_{Channel}$	= 30	m
	Width	B	= 0.5	mm

Table V-1

Considerations on equilibrium concentration

The perforated bottom implies in principle that entrainment at the bed is impossible. Hence the entrainment flux E_δ should be set to zero. The exchange process term $(E_\delta - D_\delta)$ would thus reduce to:

$$E_\delta - D_\delta = \alpha\, \omega_s(C_* - C) = \alpha\omega_s(-C) \qquad \textbf{(Eq V-3)}$$

According to the bottom boundary condition used, namely the gradient-boundary condition (see section III.2.2), E_δ depends on the equilibrium concentration C_*. This term disappears as showed in (Eq V-3). However, the capacity of the experimental dispositive to prevent entrainment is only theoretical and must be verified.

Understanding the utility of the rigid bottom part of the channel is a key aspect to interpret the behavior of the concentration profile obtained. As said in the former section, thanks to the rigid bottom, the flow develops both concentration and velocity equilibrium profile (vertically).

Let's underline the fact that it doesn't mean that the concentration at the end of the rigid section is at equilibrium. Indeed the only source of sediment is the upstream supply and doesn't necessarily satisfy the sediment carrying capacity. In other words, C_0 is not supposed to be equal to C_*. C_0 only depends on the amount of sediment provided at the inlet while C_* depends on a number of flow and sediment characteristics (Eq IV-12).

The preceding remarks on equilibrium concentration are useful to understand and interpret correctly the present case study.

Aims and assumptions

As stated in the former sections, the entrainment process is theoretically stopped by the perforated bottom. Furthermore, the experiment does not intend to simulate bed-load transport nor bed variations. As a consequence of that, only the advection-diffusion equation (Eq IV-3) is required to describe the sediment transport:

$$\frac{\partial}{\partial x}(hCU) + \frac{\partial}{\partial x}(\varepsilon\, \partial_x C) = \alpha\, \omega_s(-C) \qquad \textbf{(Eq V-4)}$$

Calculations for this test case have been reported by van Rijn (1986), Lin and Falconer (1996) and Wu, Rodi & Wenka (2000). Their objective was to analyze the concentration vertical profile over the depth.

However, in the present work, the purpose is determining the mean concentration shape along the channel. Thus, the measured concentrations available in the literature (Wang & Ribberink, 1986) have been integrated to obtain a single mean value in each station. This procedure gives an approximation of the concentration distribution along the channel.

Analytical solution

In order to reinforce the validation, an analytical solution is implemented. (Eq V-4) leads to the following solution:

$$C = C_0\, e^{-\alpha \frac{\omega_s}{U\, h} x} \qquad \textbf{(Eq V-5)}$$

where the diffusion process have been neglected. This hypothesis must be verified after the simulation is performed.

Simulation process

In order to get a uniform flow, the channel slope must balance the friction slope. From k_s, the Chézy coefficient is calculated with (Eq IV-6) and injected in Chézy's law. The value obtained are $C_{chézy}$ = 49.39 and $\partial z_b/\partial x = 0.11$ %

The calculated bed shear velocity is determined via (Eq IV-9). The value obtained is u_* = 0.034 m/s. This is in good agreement with the values of 0.035 m/s calculated by Lin and Falconer (1996) and 0.033 m/s observed in the experiment.

First, the simulation is realized using a constant value[18] for α = 1 (α is here chosen to minimize the error between measured and computed value).

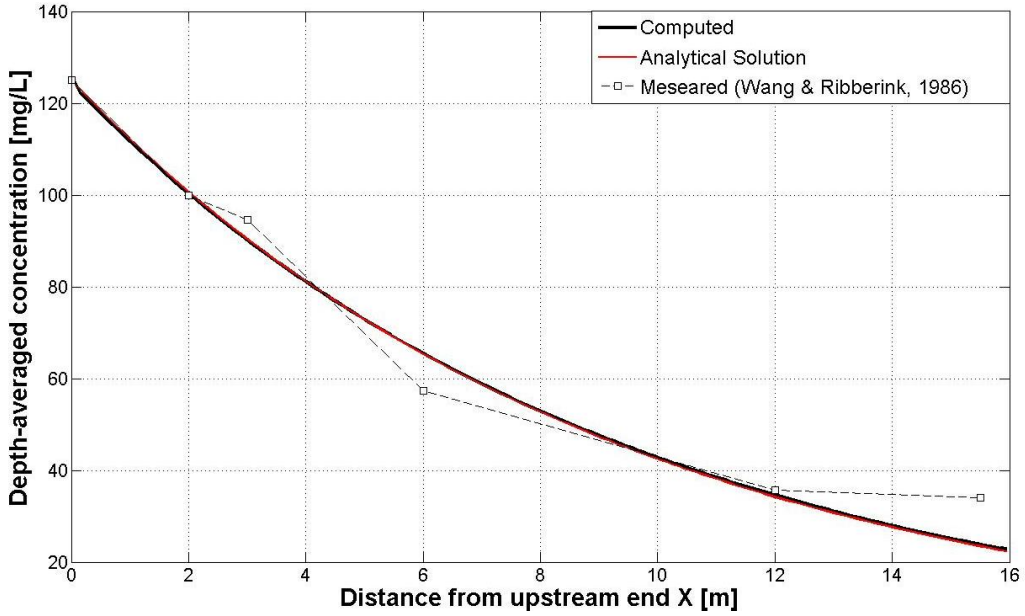

Figure V-5: Comparison of the distribution along the channel

As can be seen from Figure V-5, both computed and analytical solution are identical. That gives confidence in the performance of the model developed. However, no satisfactory results are obtained with respect to the measured concentration. Indeed both analytical and computed solution tends to the zero concentration expected while the measured results seem to stabilize after 12 meters. The representative values of each term in (Eq V-4) are:

Advection	$\frac{\partial}{\partial x}(hCU)$	$O\,(10^{-7})$
Exchange	$\alpha\ \omega_s(-C)$	$O\,(10^{-7})$
Diffusion	$\frac{\partial}{\partial x}(\varepsilon\ \partial_x C)$	$O\,(10^{-13})$

The assumption made on the diffusion process in thus justified and does not generate significant errors. In addition, as stated at the beginning of this section, all the parameters related to the experiment have been successfully compared to those found in the literature.

[18] The use of a constant value is not trivial, as explained in section V.2.3

It appears clearly to the author that imposing a zero concentration value ($C_* = 0$) is not valid in practice. In other words, entrainment is not fully prevented by the experimental dispositive. A residual suspended sediment transport is then assumed and (Eq V-4) is modified to take it into account.

Results

In Figure V-6, the black curve represents the computed concentration using $\alpha = 1.75$ and $C_* = 30$ mg/L. The latter corresponds to the measured concentration at the outlet. In order to underline the importance of considering a residual sediment concentration in the flow, the analytical solution (Eq V-5) is also computed with $\alpha = 1.75$ (red curve). Despite the parameters are all the same, the two curves are clearly different.

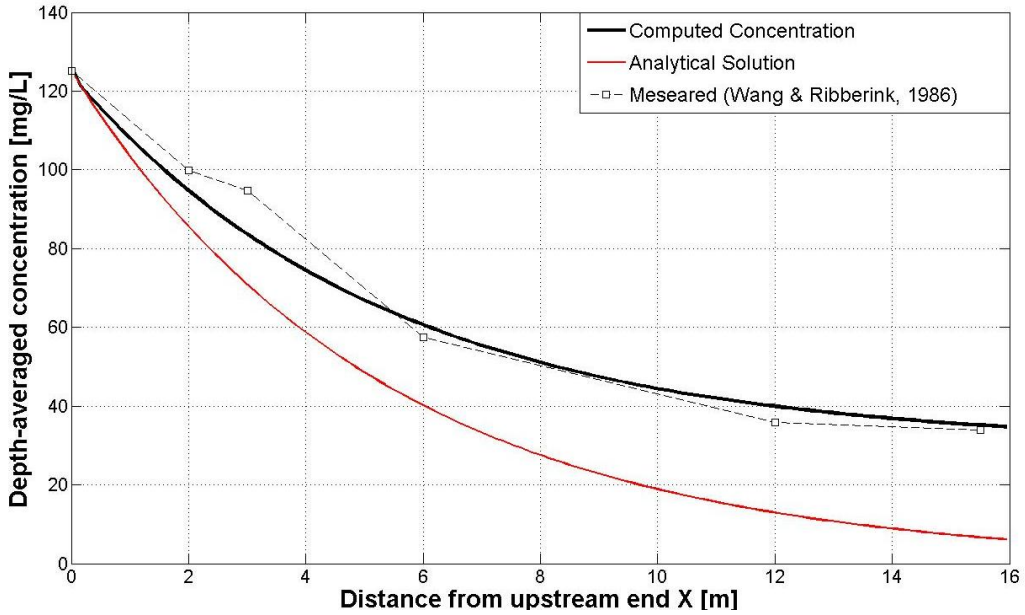

Figure V-6: Concentration along the channel: comparison

The present developments prove that the parameters and hypotheses used to model the Wang and Ribberink's (1986) experiment are relevant with respect to the present non-equilibrium situation. Indeed, the only calibrated parameter in Figure V-6 is α. The model is thus ready for further investigations on α (see Chapter VI).

V.2.2 NET ENTRAINMENT AT THE BED

Experimental configuration

This experiment (van Rijn L. , 1981) consisted in a flume with initially clear water flowed over a sand bed. In other words, no sediments were supplied at the upstream end of the inflow section. The rigid part of the channel allowed the flow to develop a velocity equilibrium profiles. The sediment concentrations were measured in a steady, uniform flow over a porous bed.

The sediments are entrained into suspension until the full transport capacity is reached. The situation is sketched in Figure V-7.

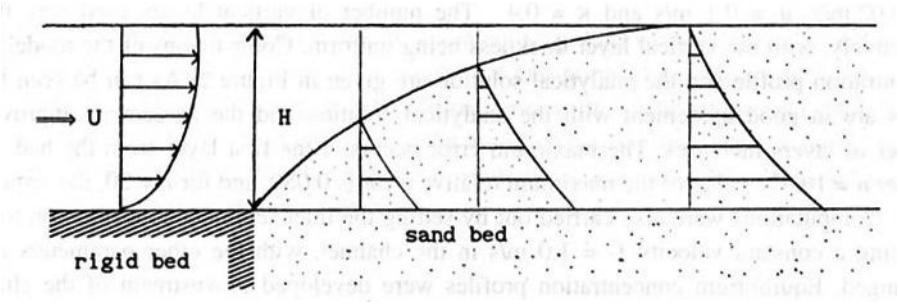

Figure V-7: Net entrainment from loose bed : Experimental configuration (Lin & Falconer, 1996)

Water samples were collected simultaneously at four locations downstream of the rigid bed to determine the spatial distribution of the sediment concentrations. At each location five water samples were taken over the depth.

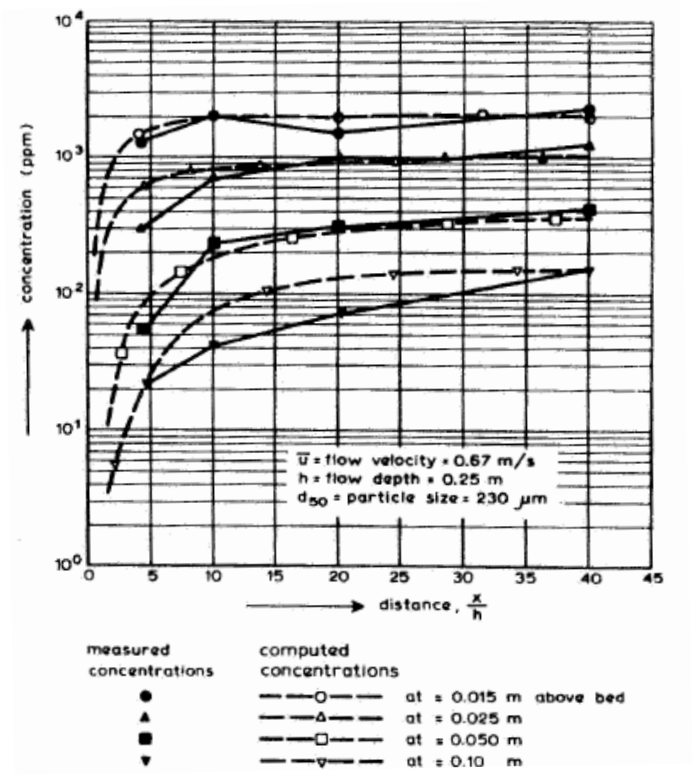

Figure V-8 : Longitudinal and vertical concentrations distribution (van Rijn L. , 1981)

Although the measuring period was made as short as possible, van Rijn (1981) reported that a small score hole was formed directly downstream of the rigid bed, thereby disturbing the flow conditions.

The complete set of data necessary to run the simulation is given in Table V-2.

	Characteristics	Values		Units
Flow	Water depth	h	= 0.25	m
	Flow velocity	U	= 0.67	m/s
Sediments	Size	D_{50}	= 0.23	mm
		D_{90}	= 0.32	mm
	Fall velocity	ω_s	= 0.022	m/s
	Density	ρ	= 2650	kg/m³
	Roughness height	k_s	= 0.01	m
	Inlet concentration	C_0	= 0	mg/L
Channel (sand bed)	Length	$L_{Channel}$	= 30	m
	Width	B	= 0.5	mm

Table V-2

At the inlet boundary, a zero-concentration profile was specified to simulate the sediment free flow.

Considerations on equilibrium concentration

The knowledge of the equilibrium depth-averaged concentration, which the flow intends to reach (after an adaptation region), is a crucial step in the present case study. However, the *prediction* of C_* is not the objective of the present simulation. For this reason, C_* was set to the value measured at the end of the channel. This results in C_* = 310 mg/L.

Aims and assumptions

As for the preceding case, the measured concentrations available in the literature (van Rijn L. , 1981) have been integrated to obtain the depth-averaged concentrations which may result in some errors.

The objective is to study the adjustment process of depth-averaged concentration. Thus, once more, bed-load transport and bed variation are not simulated. The process is then completely modeled by advection-diffusion equation.

Analytical solution

Once more, an analytical solution is implemented in order to reinforce the validation. Solving equation (Eq IV-3), in which diffusion and unsteady effects are neglected, leads to the following expression:

$$C = C_* \left[1 - e^{-\alpha \frac{\omega_s}{U\,h} x}\right] \qquad \textbf{(Eq V-6)}$$

where the diffusion process has been neglected. This hypothesis must be verified when performing the simulation.

Simulation process

Given the value of k_s (see Table V-2) the Chézy coefficient and the bed slope are calculated to ensure a uniform flow. The value obtained are $C_{chézy}$ = 39 and $\partial z_b / \partial x =$ 2.34 10^{-3} %.

Both computed and analytic solutions are compared with the laboratory results. In Figure V-9, a string disagreement is observed between the analytic solution and the computed one. It has to be noted that, in Figure V-9 the value of α has been calibrated in order to give satisfactory results for the computed solution.

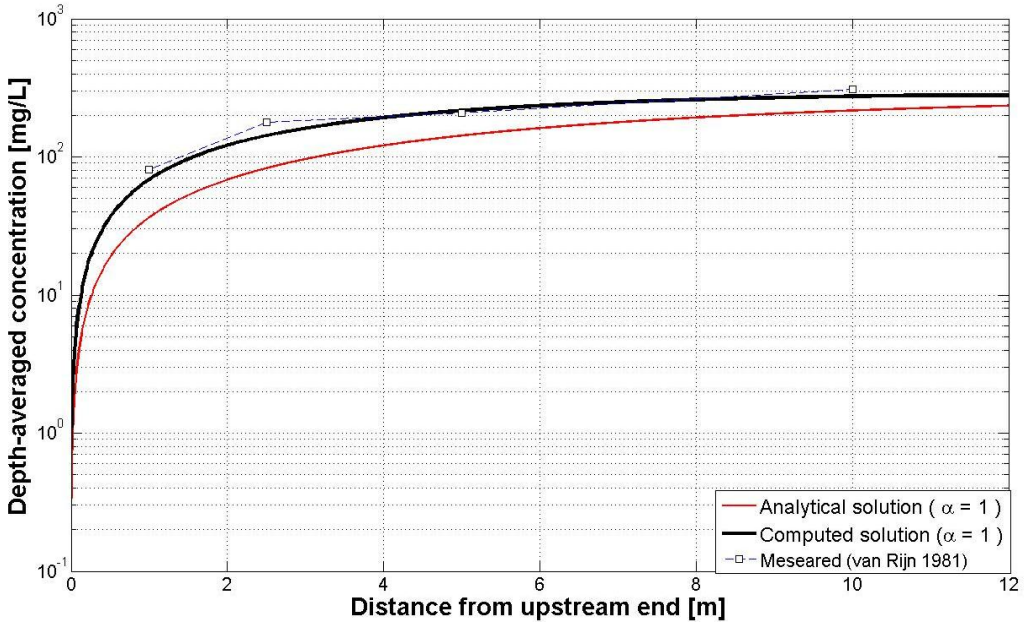

Figure V-9: Concentration along the channel: fit of the computed solution

The difference may come from the diffusion process, which is not taken into account in the analytical solution. For this reason, a comparison of the representative values for each term of the advection-diffusion equation is required:

Advection	$\frac{\partial}{\partial x}(hCU)$	O (10^{-6})
Exchange	$\alpha\ \omega_s(C_* - C)$	O (10^{-6})
Diffusion	$\frac{\partial}{\partial x}(\varepsilon_s\ \partial_x C)$	O (10^{-11})

The figures obtained prove that once more, the diffusion process is not prominent. Therefore, its contribution is not responsible for the present problem.

In Figure V-10, the chosen value of α is calibrated in order to bring satisfactory results for the analytical solution.

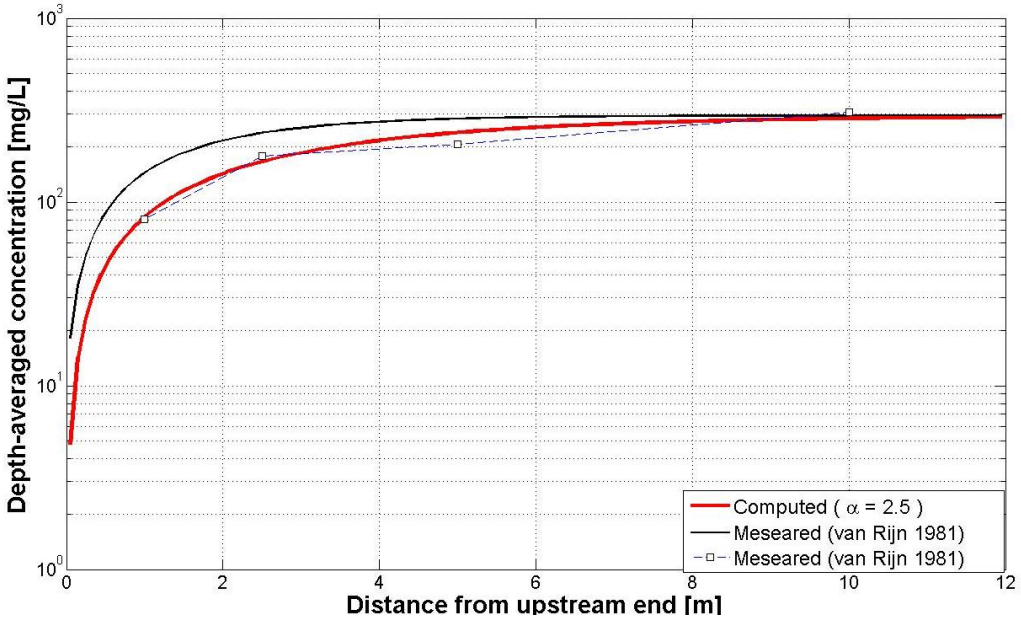

Figure V-10: Concentration along the channel: fit of the analytical solution

In section VI.3, both analytical and numerical solutions are compared quantitatively.

V.2.3 DREDGED TRENCH EXPERIMENT

Experimental configuration

The present experiment was carried out at the Delft Hydraulics Laboratory (1980). This experiment consisted of allowing a flow with fully developed sediment concentration profile flow over a gentle-sided trench. After 7.5 h, the bed level was measured. The data set of the experiment is reported in Table V-3:

	Characteristics	Values		Units
Flow	Water depth	h	= 0.0.39	m
	Flow velocity	U	= 0.51	m/s
Sediments	Size	D_{50}	= 0.16	mm
		D_{90}	= 0.2	mm
	Fall velocity	w_s	= 0.013	m/s
	Density	ρ	= 2650	kg/m³
	Roughness height	k_s	= 0.0265	m
	Inlet concentration	C_0	= 150	mg/L
Channel (sand bed)	Length	$L_{Channel}$	= 30	m
	Width	B	= 0.5	mm
Trench	Slope	10		%
	Depth	15		cm

Table V-3

Simulation process

The Chézy coefficient corresponding to the experiment has been first calculated from k_s : $C_{Chézy} = 40$.

The water depth given in Table V-3 is measured at the inlet of the channel. Consequently, the water depth at the outlet, which is the downstream boundary condition of the hydrodynamics model, is set to 0.37 m.

The equilibrium concentration as well as the adaptation coefficient must be evaluated for the present simulation. In the former cases, constant values were used for C_* and α. That was justified given that the hydrodynamics conditions, the sediment parameters as well as the bed level were kept constant. These assumptions are not valid anymore.

The inlet concentration, C_0 is considered to be at equilibrium. Thus, the equilibrium concentration formula (Eq IV-12) can be calibrated using (Eq IV-13). This results in $k = 0.0098$ and $m = 0.835$. Guo and Jin (2001) found $k = 0.0097$ and $m = 0.84$ which confirms the calculated values. Consequently, the equilibrium concentration can be calculated along the channel using (Eq **IV-12**).

However, the purpose of this section is to validate the sediment transport model. This model is used in Chapter VI to evaluate the formulations of the adaptation coefficient (see section III.4). Consequently, as for the preceding cases, the adaptation coefficient is once more imposed as a constant value. This value, $\alpha = 15$, is chosen to fit the measured bed level.

Results and validation

Using these values in the developed model, the simulated bed variation is plotted against the measured data as shown in Figure V-11.

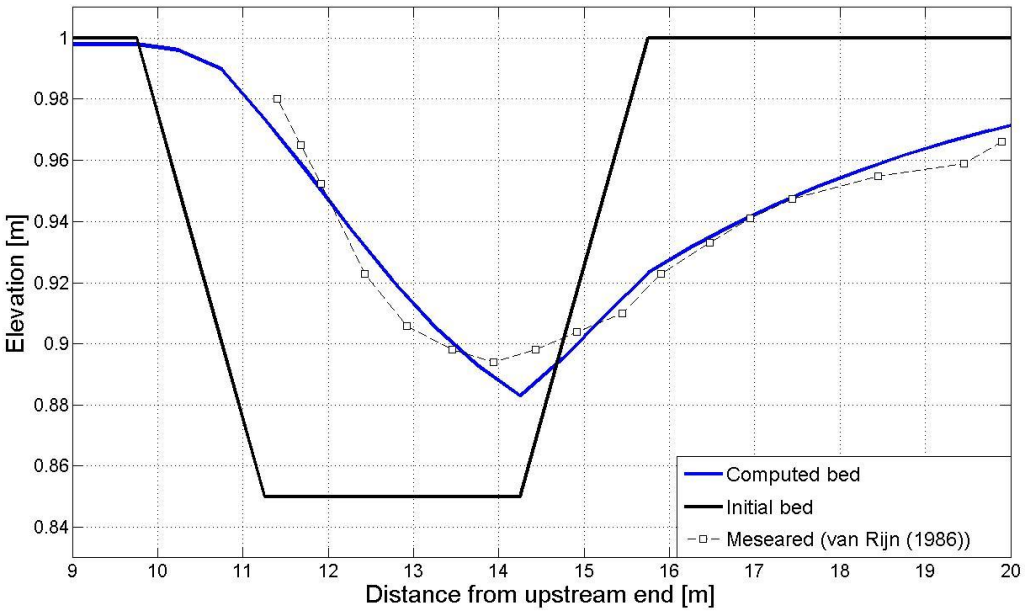

Figure V-11 : Filling of a trench dredged across a channel

Numerical results agree reasonably well with the experimental data. This last experience brings the conclusion that the suspended-load transport model can deal with bed variation. Further investigations on that experiment are held in section VI.4.

VI. EVALUATION OF EXCHANGE MODELS

Section III.4 exposes the different formulation of the adaptation coefficient while chapter IV details the construction of a 1-D numerical model for suspended sediment transport. The model has been coded successfully and validated in Chapter V. Nevertheless, some doubts still exist about the net entrainment experiment (see V.2.2). This problem is studied in detail in section VI.3.

In this chapter, the flow and sediment transport model is run with different adaptation laws (i.e. exchange models) for a number of documented benchmarks (detailed in Chapter V). The purpose is to compare the exchange model performances and then develop guidelines on which exchange model should be used or not depending on the case (according to hydraulic parameters and sediment properties).

VI.1 VALIDITY OF THE STUDY

In section III.4.3, five parameters are isolated to express the four adaptation laws:

$$\alpha = f\left(u_*, \omega_s, h, C_{ch\acute{e}zy}, \delta\right) \qquad \textbf{(Eq VI-1)}$$

The procedure of validation performed in Chapter V leads to the conclusion that the key parameters in (Eq VI-1), are correctly calculated for each case study. Therefore, the adaptation laws computed in the following paragraphs don't suffer from major errors due to these parameters. Secondly, as the values of these parameters are fixed, the influence of α can be correctly isolated.

VI.2 PERFORATED BOTTOM CASE

VI.2.1 SENSITIVITY ANALYSIS

In the perforated bottom case, detailed in section V.2.1, the value of α is fitted to minimize the error with respect to the measured concentration.

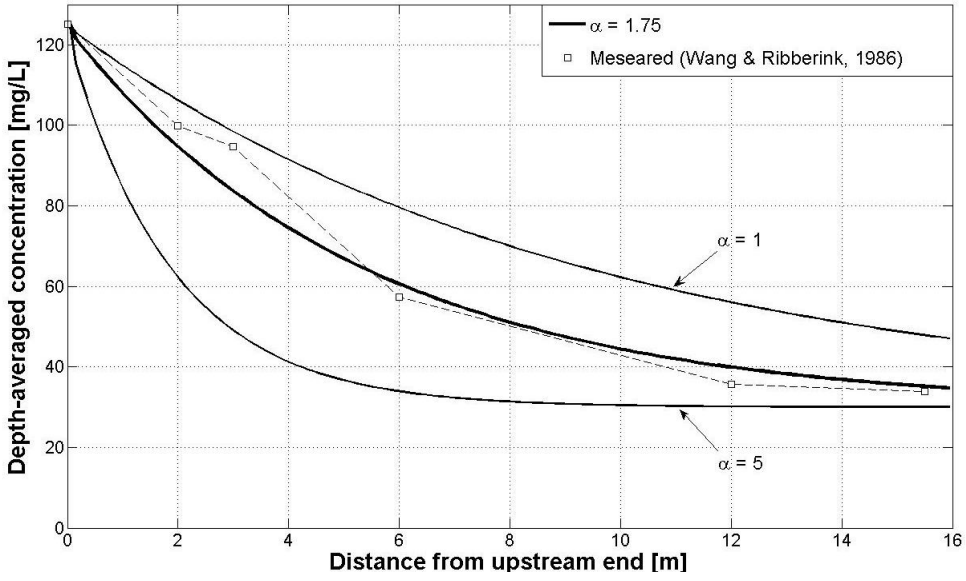

Figure VI-1: Concentration along the channel: influence of the adaptation coefficient

In Figure VI-1, the sensitivity of the concentration distribution along the bed to α is shown.. A larger value of α accelerates the process of adjustment of the concentration while a smaller value leads to the opposite observation.

The adaptation coefficient clearly rules the distance needed for the concentration to reach equilibrium.

VI.2.2 EVALUATION AND OBSERVATION

The four laws detailed in section III.4.2 have been tested for the present case study.

Each law defines δ in a different way (see Table III-1). However, for Guo & Jin's law, δ must be estimated (1999). For this reason, the dependence of α with respect to $\eta = \delta / H$ is studied in the present particular situation (Figure VI-2).

As stated in section V.2.1, a satisfactory value for α must be situated around 1.75. However, the minimum of the curve calculated doesn't approach much that ideal value, even for high η. Consequently, the value of η_δ is chosen in the range suggested by Guo & Lin (1999): $\eta_\delta = 0.01$ and $\eta_\delta = 0.1$ (see Table III-1).

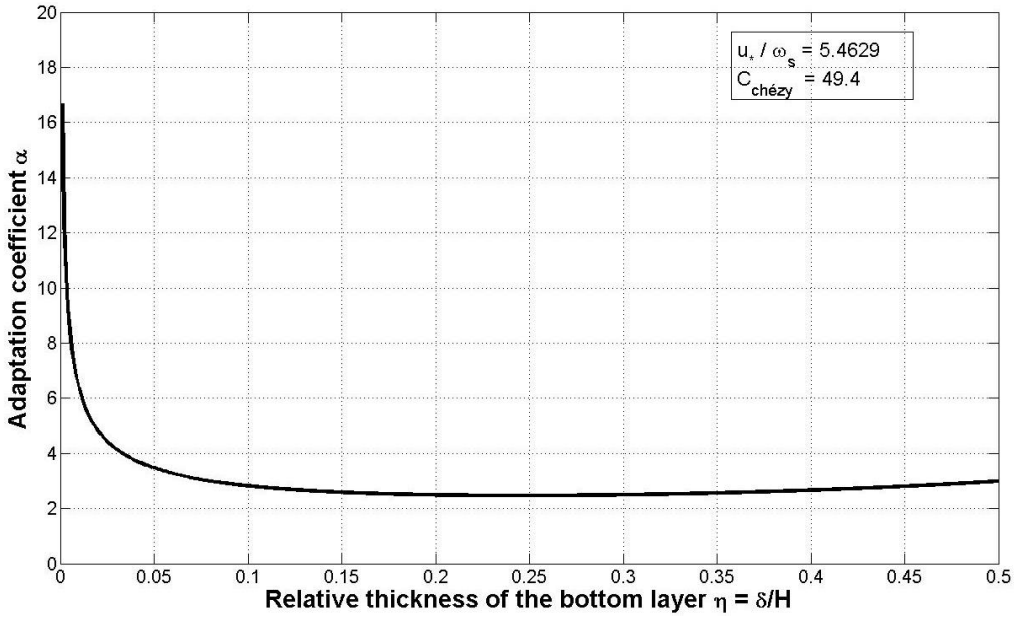

Figure VI-2: Evolution of Guo & Jin's α with respect to η

The coming Figure VI-3 compares the different concentration curve obtained for each adaptation law.

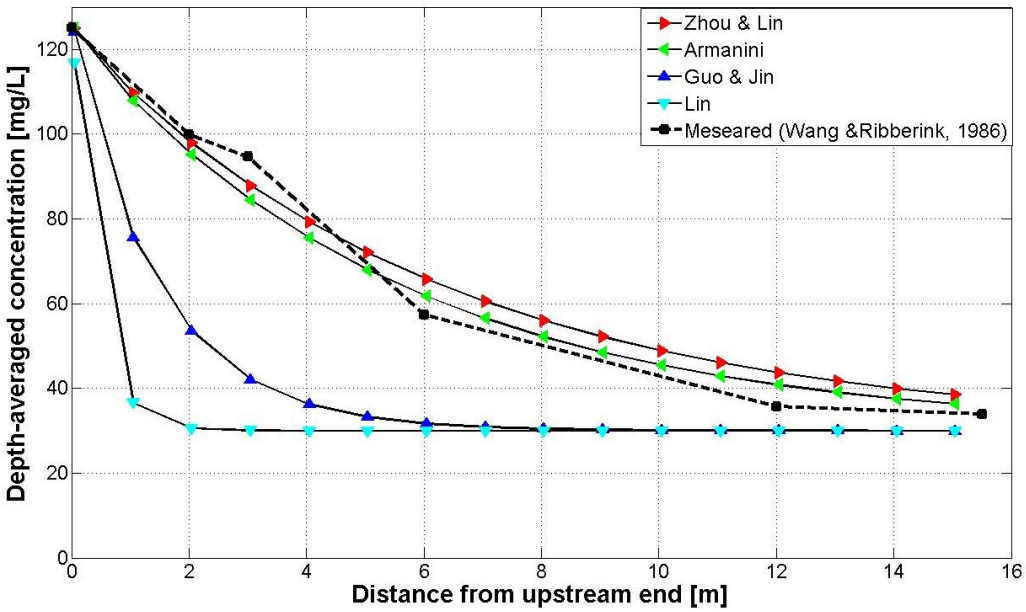

Figure VI-3: Comparison of the adaptation laws for the perforated bottom experiment

As can be seen from Figure VI-3, the results obtained are pleasingly different according to the law used. In order to quantify their accuracy, the error is calculated in three different ways (see annex p.78). The results are summarized in Table VI-1.

	δ [cm]	η	α	L_s [m]	*BIAS* [mg/L]	*AGD*	*RMS* [mg/L]
Zhou and Lin	/	/	1.49	12.39	2.15	1.093	5.72
Arm.-Di Silvio	0.41	0.019	1.68	11.02	-0.28	1.074	5.22
Guo and Jin	0.215	0.010	6.35	2.92	-22.26	1.468	30.22
Lin	0.019	8.8 *e*-4	24.90	0.74	-29.81	1.745	40.48

Table VI-1

From Table VI-1and Figure VI-3 it can be observed that:

1) The calculated adaptation coefficient is always larger than 1.
2) Armanini & Di-Silivio's and Zhou & Lin's curves are very close and give the best results.
3) For those laws, the prediced adaptation lengths are well estimated compared with the measured profile.
4) The difference between the two curves is constant along the channel

These observations are interpreted in section VI.5.

VI.3 NET ENTRAINMENT AT THE BED

This case is, to a certain extent, problematic in the present work. Indeed, in section V.2.2, it has been shown that computed and analytic solutions give different solutions for the same value of α. This problem is address in the next paragraphs.

VI.3.1 SENSITIVITY ANALYSIS

As for the preceding test, the sensitivity analysis illustrates one of the key aspects of the adaptation coefficient: its influence on the rate of adjustment in non equilibrium situation.

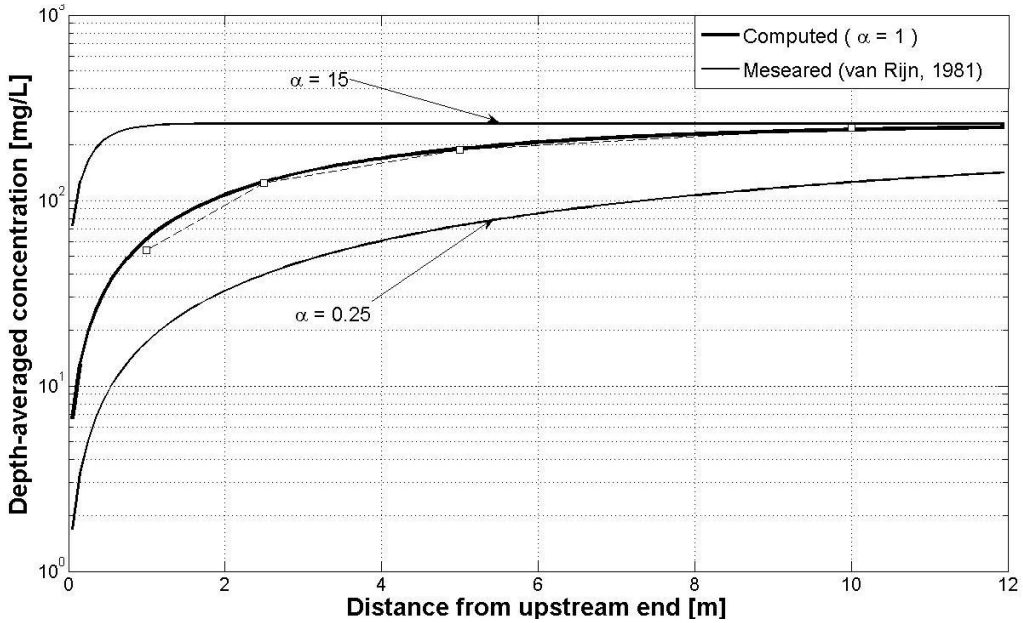

Figure VI-4: Concentration along the channel: influence of the adaptation coefficient

VI.3.2 COMPARISON OF BOTH NUMERICAL AND ANALYTICAL SOLUTION

For the present case study, the problem remains to know which one is problematic: the analytical solution or the computed one? This problem couldn't be sorted out in the validation part of this work (section V.2.2). Indeed according to the value of α (chosen arbitrary) both formulations had the possibility to match or not the experimental data.

This section deals with the presented formulations for α (see Table III-1). Consequently, the computed values of α are not subjective anymore. Therefore, the performances of the two solutions of the advection-diffusion equation can be evaluated.

For the case studied, the sediment number $\omega_s/u_* = 0.4106 > 0.1$, which invalidates Lin & al's law, as explained in section III.4.2. For Guo & Jin's law, η_δ = 0.01 as prescribed in Table III-1.[19]

[19] The dependence of α with respect to η_δ has the shape as for the preceding test. Even for an unrealistically large value of η_δ, α remains larger than 5. For this reason, it is set to the maximum value in the range prescribed by Guo & Lin (1999).

Qualitative comparison

Both analytical and numerical solutions are sketch in Figure VI-5 and Figure VI-6 respectively

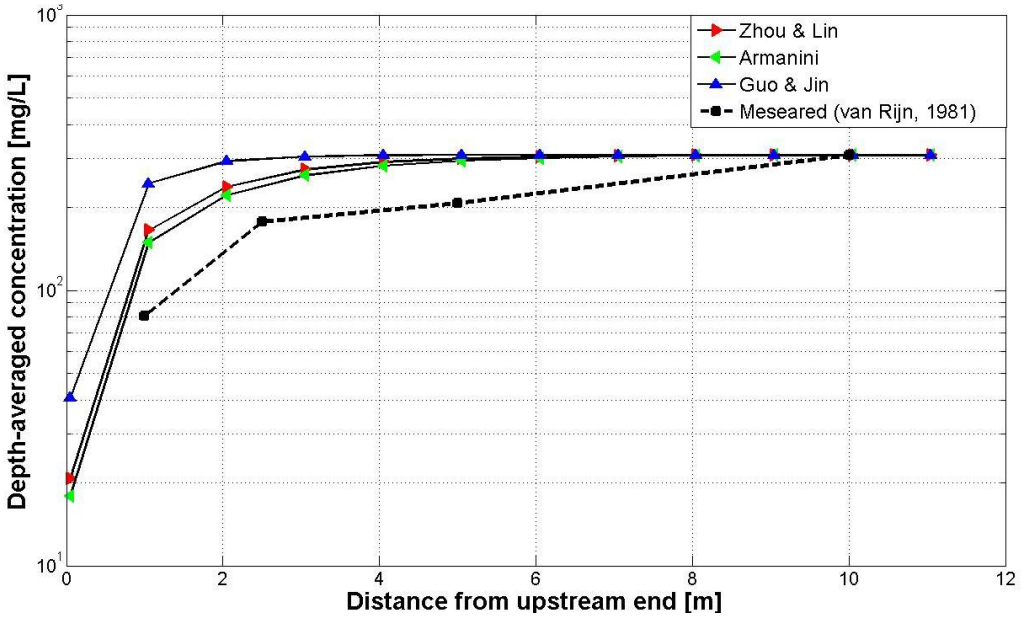

Figure VI-5: Adaptation laws: comparison of the numerical model solutions

In Figure VI-5, it can be qualitatively stated that none of the curves satisfy flume measurement. However, the analytical solution reveals that Zhou & Lin's solution as well as Armanini & Di Silvio's one perfom well. It seems obvious that the analytical solution gives better results than the other one.

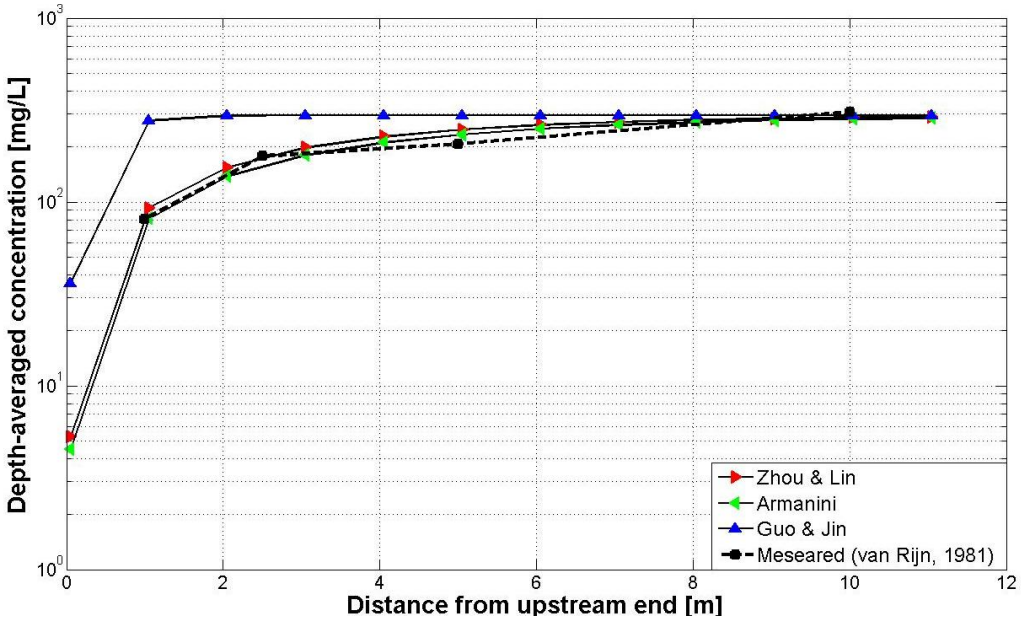

Figure VI-6: Adaptation laws: comparison of the analytical solutions

Quantitative comparisons

Some key values are contained in Table VI-2 and Table VI-3. In order to evaluate the goodness-of-fit, three statistical parameters are used (see annex p.78).

	δ [cm]	η	α	L_s [m]	*BIAS* [mg/L]	*AGD*	*RMS* [mg/L]
Zhou and Lin	/	/	2.73	2.78	63.24	1.43	73.09
Arm.-Di Silvio	0.018	0.072	2.33	3.26	53.98	1.36	63.05
Guo and Jin	0.250	0.010	19.9	0.38	115.64	1.778	140.64

Table VI-2: Numerical key parameters and error calculation

	δ [cm]	η	α	L_s [m]	*BIAS* [mg/L]	*AGD*	*RMS* [mg/L]
Zhou and Lin	/	/	2.73	2.78	15.83	1.11	27.07
Arm.-Di Silvio	0.018	0.072	2.33	3.26	2.98	1.01	20.20
Guo and Jin	0.250	0.010	19.9	0.38	110.65	1.74	13.29

Table VI-3: Analytical key parameters and error calculation

Conclusion

The value contained in both herein tables reinforce the qualitative comparison of Figure VI-5 and Figure VI-6. The model is unable to reproduce faithfully (at least less than the analytical solution) the phenomenon of adjustments when strong entrainment is involved. However, the shapes of the curve are in agreement with the solution. In addition, extreme situations like the one studied are not present in all sediment transport processes.

VI.3.3 COMPARISON OF THE ADAPTATION LAWS

Whatever the way to reproduce the experiment, the following observations can be formulated:

1) The calculated adaptation coefficient is always larger than one
2) Armanini & Di-Silivio's and Zhou & Lin's curves are once more very close from each other and give the best results, espacially in the analytical solution (Table VI-3).
3) For these two laws, the prediced adaptation lengths are well estimated with respect to the measured profile.

The observation are the same as in the preceding test. That gives a guideline for the general interpetations (see section VI.5).

VI.4 MIGRATION OF A TRENCH

VI.4.1 INTRODUCTION

In the migration of the trench experiment detailed in section V.2.2, a value of α = 15 is used to validate the model. For that value, the initial and final computed bed as well as the measured bed elevation are sketched in Figure VI-7. Similarly, the corresponding initial and final sediment carrying-capacity as well as the computed final concentraion are compared.

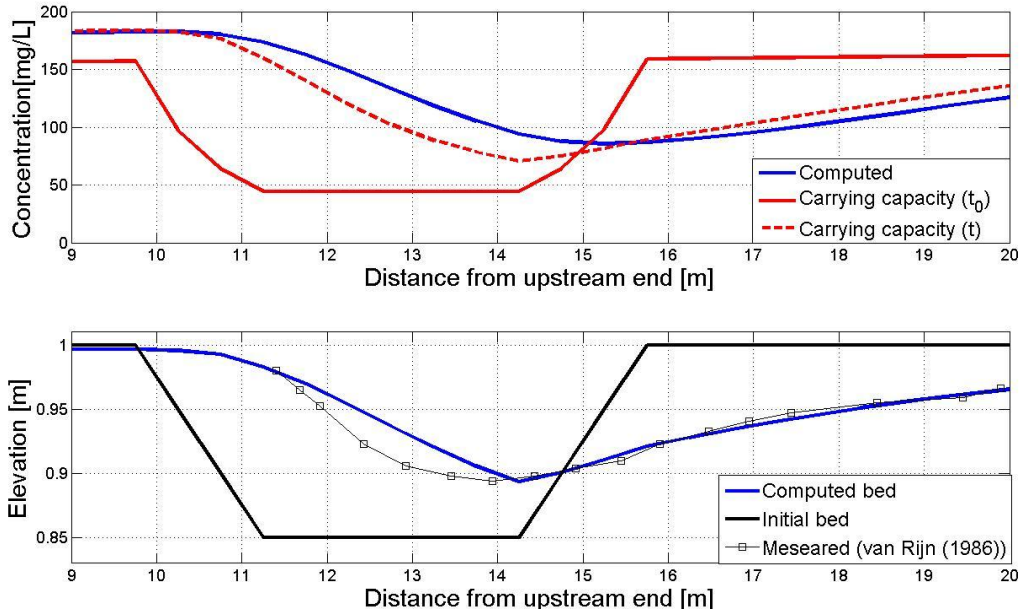

Figure VI-7: Migration of the trench: concentration and bed level evolution with α = 15

In the first part of the trench, intense deposition occurs as the computed concentration is by far larger than the equilibrium concentration. Indeed, exceding deposition is observed in that area.

On the contrary, the bed level of the right side of the trench perfectly corresponds to the laboratory results. The small difference between computed and equilibrium concentrations curves reflects this good agreement. Indeed, if the actual concentration is equal to the equilirium concentration, an equilibrium state is reached.

In that simulaltion, α was calibrated and kept constant along the channel. However this shouldn't be the case for that type of experimental configuration. Indeed, α clearly depends on the actual flow conditions (see section III.4.3). These latter change significantly as the water passes over the trench.

After a short analylisis of the influence of α on the present experiment results, benchmark adaptation coefficient are implemented to take into account the variability of the flow conditions over the dredged trench.

VI.4.2 SENSITIVITY ANALYSIS

In Figure VI-8 the influence of α on the the computed concentrations and bed levels is illustrated.

For a small value of the adaptation coefficient (α = 1), it is observed that the concentration longitudinal distribution is little affected in the region of the trench. That means that despite the great difference existing between C, the actual concentration and C_*, the equilibrium concentration, the exchange process is slowered (or not accelerated) by the small value of α. For the same reasons, the bed level changes are not significant.

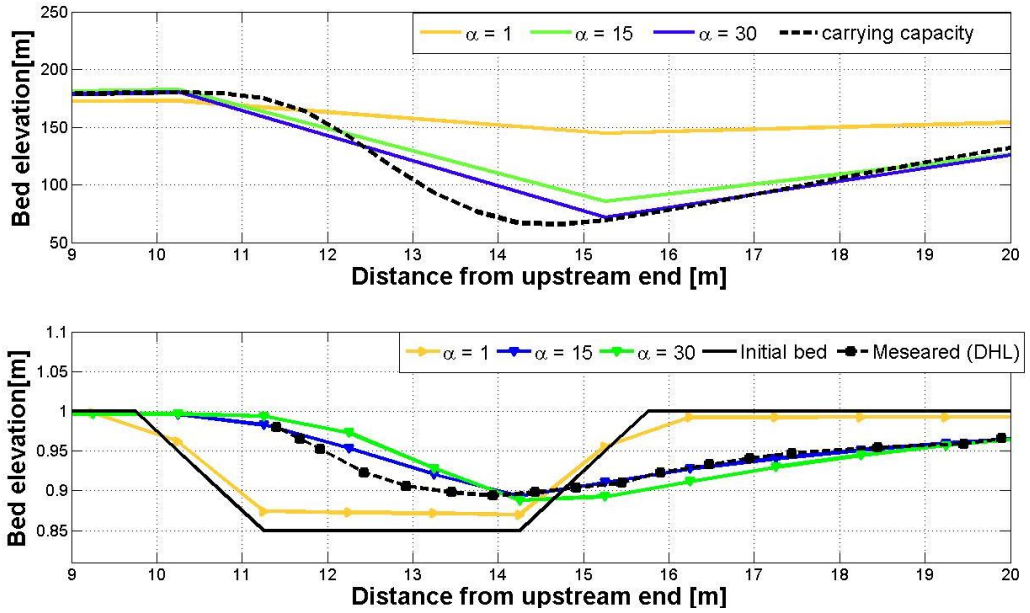

Figure VI-8: Influence of α on concentration and bed elevation

On the contrary, a large value of α accelerates the process of adjustment. However, it can be observed that in the present case, the sensitivity on the final results is smaller than that for the same reduction of α.

VI.4.3 ADAPTATION LAWS: CONSIDERATIONS

Once more, the adaptation laws are compared. The Lin & al.'s coefficient is not studied given that its inherent limited domain of applicability (see section III.4.2) prevents from using it in the present case.

In the experiment configuration, a new element must be considered. Indeed, as explained in the former paragraphs, contrary to the preceding cases study, the hydrodynamic conditions along the channel are not constant anymore. Thus the sensibility of the adaptation laws to changing flow condition can be studied.

The top part of Figure VI-9 shows the evolution of the 3 adaptation coefficients when passing over the trench. The blue curve displays much larger values than the red one and the green one. The behavior of these curves is little influenced by the trench.

The red and the green curves are very close. In order to compare the red and the green curve, a relevant zoom is also sketched.

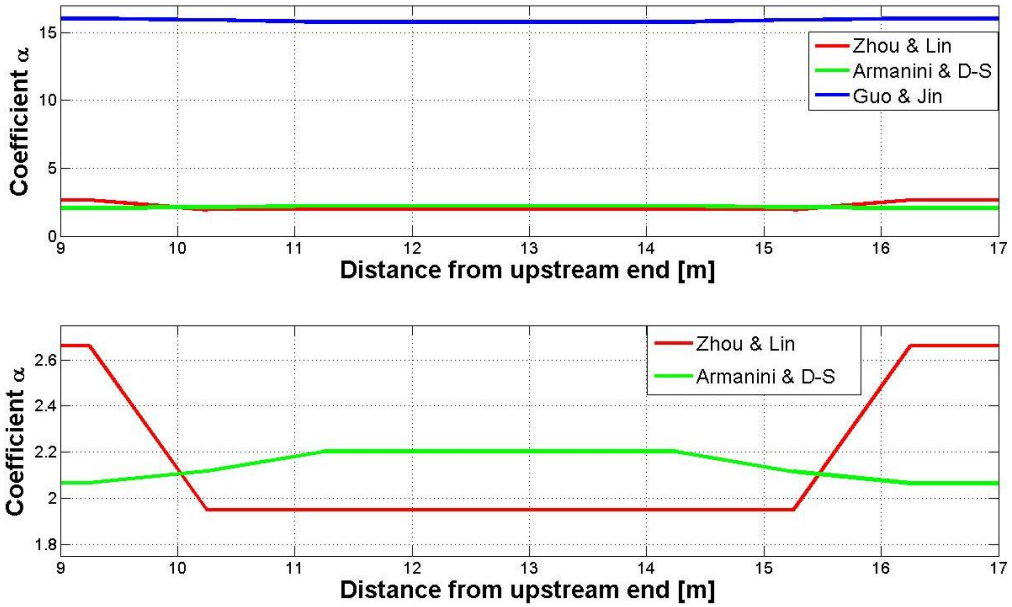

Figure VI-9: Adaptation coefficient along the trench at simulation end

In Figure III-8, it is shown that Armanini & Di Silvio's law behave similarly. However they tend to separates for high value of the Rouse number.

When passing over the trench, the flow is slowed as the Chézy coefficient increases. These effects reduce the value of the friction velocity (Eq IV-9) which in turn increases the sediment number. That explains the increasing difference toward the middle of the trench.

According to Figure VI-9, one can predict, thanks to Figure VI-8, that the value of α for the green and the red curve are too small to simulate exchange process correctly.

However the Guo and Jin's formula displays values in the range of the constant value (α = 15) used to fit the experiment.

VI.4.4 ADAPTATION LAWS: COMPARISON

Figure VI-10 shows the simulation results.

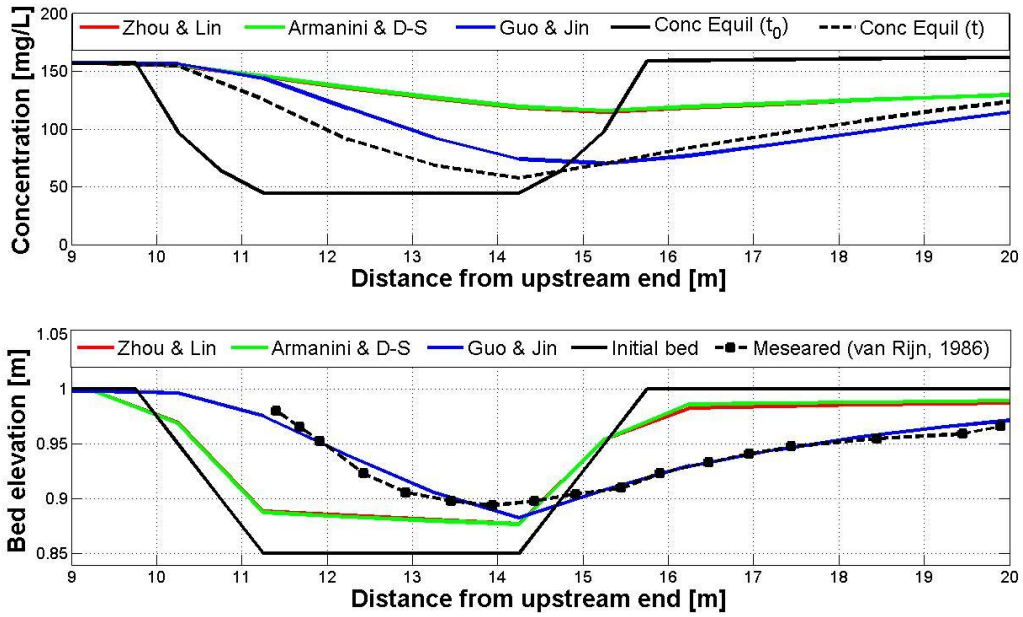

Figure VI-10: Adaptation laws: comparison of bed elevation and concentration at simulation end

From the preceding paragraphs the following observations can be formulated:

1) The adaptation coefficients varies with respect to flow conditions, staying larger that one.
2) In the present case study, that variation does not provocates significant changes on the final results.
3) Armanini & Di-Silivio's and Zhou & Lin's curves are still identical. The small relative variations are caused by the changing flow conditions which affect the sediment number
4) Zhou & Lin's law display different comportment for erosion and deposition, both active process in that simultaion. However, that difference is not highlighted by the present experimental dispositive.
5) Guo and Lin's law shows very good agreement in the present simultation

VI.5 INTERPRETATION AND CONCLUSIONS

In all the experiment described in this chapter, the adaptation coefficient is always larger than 1. The adaptation coefficient is intrinsically defined as the link between the near bed concentration and the depth-averaged concentration, both in equilibrium state or not. This relation expressed by their ratio. Thus, as the near bed concentration is always larger than that in the flow, $\alpha > 1$.

The influence of α has been illustrated in many configurations. Its role in the adjustment process has been clearly highlighted by conducting a sensitivity analysis for all the cases considered, using a different spatially constant values.

Using a constant value for α is a current practice in sediment transport modeling. This assumption is valid for the perforated bottom experiment as well as for the net entrainment one. Indeed, in these particular cases the flow conditions are constant. In section III.4.2, it was been shown that whatever the definition of α, the formulation always depends on these conditions.

For this reason, the assumption of a spatially constant α is theoretically non valid in the moving trench experiment. The adaptation coefficient's sensitivity to these changes was thus examined at the trench level, where the flow conditions are mostly modified. No significant changes were observed with respect to the value of α nor the final bed elevation. It is thus concluded that the assumption of a constant value for α is justified when flow perturbations are not significant.

The diffusion process, even crucial for suspended sediment transport was estimated negligible for all the case of study.

Lin & al's law was unsuccessfully tested in all the simulations. Indeed, given its narrow domain of application, this efficiency of this law was not illustrated in this master thesis.

Armanini & Di Silvio and Zhou & Lin's formulations have showed a similar behavior in most cases. When increasing the value of the Rouse-Type number, that is in changing flow conditions, their divergences was underlined and explained.

These two laws were particularly accurate to simulate the two first experiment where the required value for α was quite low [0-3]. Their predictive power (no calibration) makes them very powerful for such situations.

Guo & Lin's law has proved to perform well in the dredge trench experiment. This experiment considered a fully developed concentration and velocity profile at the level of the trench. These are typically the assumptions made to formulate Guo & Jin's adaptation coefficient law, which explain their accuracy to model this case study.

However the latter formulation, if compared with others, contains an important weakness. Indeed, because the reference level is not formulated, this parameter need to be calibrated which reduce substantially potential

VII. CONCLUSIONS

Exchange models are one of the most important aspects for sediment transport models. Poor knowledge about sediment transport capacity and adaptation coefficient formulations, both components of most exchange models, causes uncertainty and reduces the predictive power of such models. This master thesis intends to bring a critical comparison of existing adaptation coefficient formulations.

An intensive literature review was conducted to gather background information over this complex subject. Subsequently, the relevant parameters were isolated in these formulations and a sensitivity analysis has been carried on in order to dominate them.

In order to reinforce this critical analysis, a 1D mathematical model to simulate non-equilibrium transport has been established. The latter has been validated confronting it to a wide range of existing literature example including numerical simulations, analytical solutions and laboratory data. It has been demonstrated that the present fully developed model is accurate in modeling channel bed variation under both bed-load and suspended-load transport.

However, its applicability was limited by the net entrainment experiment which illustrates its weakness to modelize special sediment transport conditions.

This still powerful tool has been used to provide a better understanding of non-equilibrium transport aspects. In addition, it has constituted the key to confront and to understand the different adaptation laws in a range of benchmark laboratory experiment.

Lin & al.'s efficiency was not illustrated in this master thesis as its domain of applicability prevented it from being used in many tests performed.

Guo & Jin's formula was successfully used in an experiment in which sediment and velocity profiles were assumed. However, its unpredictability related to the definition of the bottom layer thickness constitutes a serious weakness for sediment transport modeling.

Zhou & Lin's as well as Armanini & Di Silvio's formulation has shown good behaviour in modeling suspended sediment transport in steady uniform flow conditions where the range of variation of the adaptation coefficient was small. In addition their predictive power makes them highly attractive for sediment transport modeling.

This master thesis has involved various aspects of specific scientific areas, such as hydrodynamic and numerical modeling to finally converge to interesting, and sometime surprising results.

VIII. NOTATIONS

$(\Gamma_s \ \partial_x C)$	=	Turbulent sediment flux
(h-δ)	=	Thickness of the suspended-load transport layer
c_{δ_*}	=	Near-bed equilibrium sediment concentration at δ over the bed
c_δ	=	Near-bed concentration at δ over the bed
u_*	=	Friction velocity
γ_s	=	Specific weight of sediment
λ_{max}^{exact}	=	Biggest eigenvalue of the linearized spatial operator
ξ_M	=	Roughness parameter
$\partial/\partial t\ (z_b)$	=	Bed change rate
B	=	Channel width
c	=	Local suspended-load volumetric concentration
C	=	Depth-averaged suspended-load concentration
C_*	=	Equilibrium depth-averaged concentration
c_b	=	Calculated near-bed concentration
c_{b*}	=	equilibrium near-bed concentration
$C_{Chézy}$	=	Chézy coefficient
$c_{\delta*}$	=	Equilibrium near-bed concentration
d	=	Representative size of the particles or sieve diameter
D	=	Deposition flux
d_{50}	=	Median particle size
D_{si}	=	Dispersion sediment flux in i-direction
D_δ	=	Sediment deposition flux (downward)
E	=	Entrainment flux
e_b	=	Bed-load sediment transport efficiencies
e_s	=	Suspended sediment transport efficiencies
E_δ	=	Sediment entrainment flux (upward)
Fr	=	Froude number
G	=	Specific gravity of sediment
g	=	Gravitational acceleration
h	=	Flow depth
J	=	Friction-slope
$k\ and\ m$	=	Calibration coefficients of sediment carrying capacity formula
L	=	being the differential spatial operator
L_b	=	Adaptation length of bed-load
L_s	=	Adaptation length for suspended-load transport
n	=	Manning's coefficient
p	=	Porosity
q_b	=	Bed-load transport rate

q_b	=	Transport capacity under the equilibrium condition (q_{b*})
q_s	=	Suspended-load transport rate
R	=	Rouse-type number
R_h	=	Hydraulic radius
s	=	Specific gravity
$s^{(1)}$ *and* $s^{(2)}$	=	Sub-step of Runge-Kutta method
S_0	=	Bed-slope term
S_j	=	Channel flow resistance term
s^t	=	Known value of *s* at time *t*
s^{t+1}	=	Unknown value of *s* at time *t+1*
u	=	Flow velocity
U	=	Depth-average velocity
u_*	=	Shear velocity
u, v, w	=	Components of mean velocity
v	=	Kinematic viscosity of water
x-, y- , z-	=	Directions
z_0	=	Zero-velocity distance
z_b	=	Bed elevation
Z_R	=	Rouse-type number
z_s	=	Water surface elevation
α	=	Adaptation coefficient
α_{bk} *and* α_{by}	=	Direction cosines of bed-load movement
α_c	=	Adaptation coefficient for deposition
α_c	=	Adaptation coefficient for entrainment
δ	=	Thickness of the bed-load layer
δ	=	Thickness of the bottom layer
ε_s	=	Dispersion coefficient (also written Γ_s)
η	=	Relative flow depth
η_b	=	Reference relative flow depth
κ	=	von Kármán constant
ρ_s	=	Sediment density
ρ_w.	=	Density of water
ω_s	=	Particle settling velocity
$i = \partial z_b/\partial x$	=	Bed slope
γ	=	Specific weight of clear water

IX. REFERENCES

Armanini, A., & Di Silvio, G. (1988). A one-dimensional model for the transport of a sediment mixture in non-equilibrium conditions. *Journal de recherches hydrauliques , 26* (3).

Armanini, A., & di Sivio, G. (1986). Discussion on the paper 'A depth-integrated model for suspended sediment transport' by G. Galappatti and C.B. Vreugdenhil. *Journal of Hydraulic Research* , pp. 437-441.

Bagnold, R. (1966). An Approach to the Sediment Transport Problem From General Physics. *U.S. General Survey* .

Bagnold, R. (1973). The nature of saltation and of bed load transport in water. *Proc., Royal Soc.* London.

Brooks. (1972). *Sedimentation Engineering.* (V. Vanoni, Éd.)

Chen, D., Acharya, K., & Stone, M. (2010). Sensitivity analysis of non-equilibrium adaptation parameters for modeling mining-pit migration. *Journal of Hydraulic Engineering* .

Delft Hydraulics Laboratory. (1980). *Computation of Siltation in Dredged Trench.*

Di Sivio, G., & Armanini, A. (1981). Influence of the upstream boundary conditions of the erosion-deposition processes in open channel. *XIX IAHR Congress.* New Delhi, India.

Einstein. (1977). *Sediment transport technology.* (D. Simons, & F. Senturk, Éds.) Water Ressources Publications.

Engineering, W. U. (1959). Investigation on sediment-carrying capacity in the middle stream of Yangtz River. *Journal of Sediment Research , 4* (2), pp. 54-73.

Fäh, R. (1997). *Numerische simulation der Strömung in offenen Gerinnen mit beweglisher sohle.*

Galappatti, G., & Vreugdenhil, C. (1985). a depth-integrated model for suspended sediment transport. *Journal of Hydraulic Research , 13* (4).

García, M. a. (1991). Entrainment of Bed Sediment into Suspension. *Journal of Hydraulic Engineering* , pp. 414-435.

Graf, H. W. Fluvial Hydraulics. (p. 356). Flow and transport processes in channels of simple geometry: Wiley.

Guo, Q.-C., & Jin, Y. (1999). Estimanting the adjustement coefficient used in nonequilibrium sediment transport modelling. *Proc. Annual Conf. Canadian Society for Civil Engineering, II*, pp. 217-226.

Guo, Q.-C., & Jin, Y.-C. (2001). Estimating Coefficients in one-dimensional depth-average sediment transport model. *Canadian Journal of Civil Engineering* (28), pp. 536-540.

Guo, Q.-C., & Jin, Y.-C. (1999). Modeling sediment transport using depth-average and moment equations. *ASCE Journal of Hydraulic Engineering* (125(12)), pp. 1262-1269.

Han, Q. (1980). A study on the nonequilibrium transport of suspended sediment. *1st Int. Symp. on river sendimentation.* Beijing, China.

Lin, B. L., & Falconer, R. A. (1996). 'Numerical modelling of threedimensional suspended sediment for estuarine and coastal waters.'. *Journal of Hydraulic Research* , pp. 435-456.

Lin, B., Huang, J., & Li, X. (1983). Unsteady transport of suspended load at small concentration. (ASCE, Éd.) *Journal of Hydrauliics Engineering* .

Lin, P., Huang, J., & Li, X. (1983). Unsteady transport of suspended load at small concentration. *Journal of Hydraulic Engineering , 109(1)*, pp. 86-98.

MacArthur, R. N. (2007). *Sedimentation Engineering Chapter 1, Overview of sedimentation Engineering.* (M. H.García, Éd.)

Minor, H.-E., Altinakar, M., Bezzola, G., de Casare, G., Fäh, R., Graf, W., et al. (1999). *Transport de matière.* EPFL.

Rouse, H. (1937). Modern conceptions of the mechanics of turbulence. *Transaction, American Geophysical Union* , pp. 463-543.

Rubey, W. (1933). Equilibrium condition in debris-laden streams. *Transaction, American Geophysical Union, 14th Annual Meeting*, (pp. 497-505).

Shen, H. (1984). Two-D flow with sediment by characteristics method. (ASCE, Éd.) *Journal of Hydraulics Engineering* .

Simons, D., & Senturk, F. (1992). Sediment transport technolodgy- water and sediment dynamics. *Water Resources Publications* .

Spasojevic, M., & Holly, F. M. ASCE Manual and Reports on engineering practice. Dans M. H. García (Éd.), *Sedimentation Engineering* (Vol. 110, p. 707).

Spasojevic, M., & Holly, F. M. (2008). ASCE Manual and Reports on engineering practice. Dans M. H. García (Éd.), *Sedimentation Engineering* (Vol. 110, p. 707).

van Rijn, L. C. (1993). *Principle of sediment transport in rivers, estuaries, and coastal seas.* Aqua publications.

van Rijn, L. C. (1984b). Sediment Transport, Part III: Alluvial Roughness. *Journal of Hydraulics Engineering , 110* (12).

van Rijn, L. C. (2007, June). Unified View of Sediment Transport by Current and Waves I : Initiation of motion, Bed Roughness, and BedLoad Transport. *Journal of Hydraulic Engineering* , pp. 649-667.

van Rijn, L. (1984). Sediment transport. Part II : suspended load transport. *Journal of Hydrauliclc Engineering* (110(11)), pp. 1613-1641.

van Rijn, L. (1981). The development of concentration profiles in a steady, uniform flow without initial sediment sediment load. *IAHR Workshop on particle motion and sediment transport.* Rapperswil,Switzerland.

Wang, Z., & Ribberink, J. (1986). The validity of a depth-integrated model for suspended sediment transport. *Journal of Hydraulic Research* , pp. 53-66.

Wu, W. (2008). *Computational river dynamics.* Taylor & Francis Group.

Wu, W., Rodi, W., & Wenka, T. (2000). 3D Numerical Modeling of Flow and Sediment Transport in Open Channels. *Journal of Hydraulics* .

Z.Cao, P. C. (2002, December). Mathematical modelling of alluvial rivers: reality and myth, Part 2 : Special issues. *Proceedings of the institution of civil engineers, Water & Maritime Engineering 154* (4), pp. 297-307.

Zhang, Q., Zhang, Z., Yue, J., & Dar, M. (1983). A mathematical model for the prediction of the sedimentation process in rivers. *Proc. 2nd International Symposium on river Sedimentation.*

Zhou, J., & Lin, B. (1995). 2-D Mathematical model for suspended sediment-Part I: Model theory and validations. *Journal of Basic Science and Engineering* , pp. 78-79.

Zhou, J., & Lin, B. (1998). One-dimensional mathematical model for suspended sediment by lateral integration. *Journal of Hydraulic Engineering* .

Zyserman-Fredsøe. (1991). Data analysis of bed concentration of suspended sediment. *Journal of Hydraulics Engineering* , pp. 1021-1042.

X. ANNEX

Evaluating goodness-of-fit (Chen, Acharya, & Stone, 2010)

The goodness-of-fit between computed and measured bed elevations were evaluated by three statistical parameters include the Bias, the Average Geometric deviation (AGD), and the Root Mean Square (RMS). Each parameter provides a measure of the goodness-of-fit between the computed and the measured bed elevation from a slightly different perspective. They are described as follows:

1) *The Bias:*

$$Bias = \sum_{j=1}^{J} (Z_{cj} - Z_{mj})/J$$

Where Z_c and Z_m are the computed and measured bed elevation, respectively, and j is the data set number. The Bias with a unit of mg/L in the study represents the arithmetic mean of the difference between computed and experimental bed elevations. A positive value of Bias is produced when the calculated bed elevations are generally higher then the observed conditions.

2) *Average geometric deviation (AGD):*

$$AGD = \left(\prod_{j=1}^{J} R\ R_j \right)^{\frac{1}{J}}, RR_j = \begin{cases} \frac{Z_{cj}}{Z_{mj}}\ for\ Z_{cj} \geq Z\_mj \\ \frac{Z_{mj}}{Z_{cj}}\ for\ Z_{cj} \leq Z_{mj} \end{cases}$$

The dimensionless parameter AGD represents the geometrical mean of the special discrepancy ration, RR_j.

3) *Root mean square (RMS):*

$$RMS = \left[\sum_{j=1}^{J} \frac{Z_{cj} - Z_{mj}}{J} \right]^{1/2}$$

The root mean square represents the quadric mean of the difference between the computed bed elevations and the measured values. RMS is especially useful when deviations are both positive and negative such as overestimation and underestimation of bed deformation in the current calculation. RMS has a unit of mg/L in this study.

These three statistical parameters (Bias, AGD, RMS) provide a comprehensive evaluation of the goodness-of-fit between the computed and measured bed elevation.